Bioorg. Med. Chem. 33 (2021) 115993

Contents lists available at ScienceDirect

Bioorganic & Medicinal Chemistry

journal homepage: www.elsevier.com/locate/bmc

Cytoprotective activities of kinetin purine isosteres

Barbara Maková [a], Václav Mik [a], Barbora Lišková [b], Gabriel Gonzalez [a,g], Dominik Vítek [b], Martina Medvedíková [b], Beata Monfort [d], Veronika Ručilová [c], Alena Kadlecová [a], Prashant Khirsariya [e], Zoila Gándara Barreiro [a], Libor Havlíček [f], Marek Zatloukal [h], Miroslav Soural [c], Kamil Paruch [e], Benoit D'Autréaux [d], Marián Hajdúch [b], Miroslav Strnad [a], Jiří Voller [b,i,*]

[a] Department of Experimental Biology, Faculty of Science, Palacký University, Šlechtitelů 27, Olomouc CZ-78371, Czech Republic
[b] Institute of Molecular and Translational Medicine, Faculty of Medicine and Dentistry, Palacký University, Hněvotínská 3, Olomouc CZ-77515, Czech Republic
[c] Department of Organic Chemistry, Faculty of Science, Palacký University, 17. listopadu 1192/12, Olomouc CZ-783-71, Czech Republic
[d] Université Paris-Saclay, CEA, CNRS, Institute for Integrative Biology of the Cell (I2BC), 91198 Gif-sur-Yvette, France
[e] Department of Chemistry, CZ Openscreen, Faculty of Science, Masaryk University, Brno, Czech Republic
[f] Isotope Laboratory, The Czech Academy of Science, Institute of Experimental Botany, Vídeňská 1083, Praha 4 CZ-14220, Czech Republic
[g] Department of Neurology, Palacký University Olomouc, Faculty of Medicine and Dentistry and University Hospital, Olomouc, Czech Republic
[h] Department of Chemical Biolology and Genetics, Centre of the Region Hana for Biotechnological and Agricultural Research, Palacký University, Šlechtitelů 27, Olomouc CZ-78371, Czech Republic
[i] Laboratory of Growth Regulators, Palacký University & Institute of Experimental Botany AS CR, Šlechtitelů 27, Olomouc CZ-78371, Czech Republic

ARTICLE INFO

Keywords:
Cytokinin
Kinetin
bioisostery – Friedreich's ataxia
Mitoprotection – familial dysautonomia
Neuroprotection

ABSTRACT

Kinetin (N^6-furfuryladenine), a plant growth substance of the cytokinin family, has been shown to modulate aging and various age-related conditions in animal models. Here we report the synthesis of kinetin isosteres with the purine ring replaced by other bicyclic heterocycles, and the biological evaluation of their activity in several *in vitro* models related to neurodegenerative diseases. Our findings indicate that kinetin isosteres protect Friedreich's ataxia patient-derived fibroblasts against glutathione depletion, protect neuron-like SH-SY5Y cells from glutamate-induced oxidative damage, and correct aberrant splicing of the ELP1 gene in fibroblasts derived from a familial dysautonomia patient. Although the mechanism of action of kinetin derivatives remains unclear, our data suggest that the cytoprotective activity of some purine isosteres is mediated by their ability to reduce oxidative stress. Further, the studies of permeation across artificial membrane and model gut and blood-brain barriers indicate that the compounds are orally available and can reach central nervous system. Overall, our data demonstrate that isosteric replacement of the kinetin purine scaffold is a fruitful strategy for improving known biological activities of kinetin and discovering novel therapeutic opportunities.

1. Introduction

Cytokinins, N^6-substituted adenines in chemical terms, are major regulators of plant growth and development but they also have activities in other organisms, including humans.[1] In plants, they occur as free cytokinin bases (the active forms) as well as ribosides and glucosides (transport and storage forms). The first studies of their pharmacological activity in humans focused on the anti-cancer activity of certain

Abbreviations: ADME, Absorption, distribution, metabolism and excretion; ATCC, American Type Culture Collection,; ATRA, All-*trans* retinoic acid; BSA, Bovine serum albumin; BSO, L-buthionine sulfoximine; DCM, Dichloromethane; DFO, Deferoxamine; DHE, Dihydroethidium; DIC, *N*,*N*'-Diisopropylcarbodiimide; DMF, *N*,*N*-Dimethylformamide; DMSO, Dimethyl sulfoxide; DMEM, Dulbecco's modified Eagle's medium; ECACC, European Collection of Authenticated Cell Culture; EDIPA, *N*-Ethyldiisopropylamine; GSH, Reduced glutathione; FA, Friedreich's ataxia; FBS, Fetal bovine serum; FXN, Frataxin; ISC, Iron-sulfur cluster; HBBS, Hank's balanced buffer solution; HOBt, 1-hydroxybenzotriazole; MW, Microwave; PAMPA, Parallel Artificial Membrane Permeability Assay; PBS, Phosphate buffer saline; PI, Propidium iodide; RED, Rapid equilibrium dialysis; R-LA, *R*-lipoic acid; TEA, Triethylamine; TFA, Trifluoroacetic acid,.

* Corresponding author at: LGR proper and Department of Experimental Biology, Palacký University & Institute of Experimental Botany AS CR, Šlechtitelů 27, Olomouc CZ-78371, Czech Republic.
E-mail address: jiri.voller@upol.cz (J. Voller).

https://doi.org/10.1016/j.bmc.2021.115993
Received 2 December 2020; Accepted 31 December 2020
Available online 6 January 2021
0968-0896/© 2021 Published by Elsevier Ltd.

cytokinin ribosides. Later research focused on cytokinin bases, for which diverse activities (including neuroprotective, antipsoriatic, and anti-aggregatory activities) have been reported, as reviewed by Kadlecová et al. in 2019.[2] In contrast to some cytokinin ribosides, cytokinin bases show no or limited toxicity toward human cells. The most intensively studied cytokinin base is kinetin (N^6-furfuryladenine), in large degree because it delays the aging of human cells *in vitro*[3] and may naturally occur in humans.[4] An important impetus for kinetin research was the discovery of its ability to correct the aberrant ELP1 and NF1 pre-mRNA splicing responsible for the neurodegenerative disorders familial dysautonomia and neurofibromatosis type I, respectively.[5,6] Follow-up studies demonstrated that kinetin can increase the abundance of ELP1 wild-type transcripts in transgenic mouse familial dysautonomia models. The first human studies demonstrated that kinetin is orally available.[7] Recently, promising *in vitro* results have been reported for combination of kinetin and phoshatidylserine.[8] Other investigations showed that kinetin has protective activity in models of Parkinson's[9] and Huntington's diseases.[10]

In plants, cytokinin signaling is well characterized, from signal recognition by plasma membrane receptors (e.g., AHK2, AHK3 and AHK4 in the model plant *Arabidopsis thaliana)* to activation of the response genes.[11] In contrast, mechanisms of action of cytokinins, including kinetin, in human cells remain largely unknown. Studies of cytokinin bases often focus on their ability to protect biological macromolecules, cells, and tissues against stress by direct antioxidant activity or induction of antioxidant defenses, as reviewed by Kadlecová et al. in 2019.[2] Recent exciting studies have shown that kinetin riboside-5′-triphosphate, a metabolite of kinetin, acts as a neosubstrate of the mitoprotective kinase PINK1[9] and CK2 kinase, which phosphorylates huntingtin aggregates.[10] Perturbance of these kinases' activities plays major roles in Parkinson's and Huntington's diseases, respectively, so restoring or modulating their activities using kinetin could provide potent novel therapeutic options.

In contrast to cytokinin ribosides, for which several series of derivatives have been reported[12–19], studies of pharmacological activities of cytokinin bases have been largely limited to naturally occurring bases. However, a correction of aberrant splicing of ELP1 by 2-chlorokinetin[20] and some 6,8-disubstituted purines[21] was reported and it was also demonstrated that 9-substituted derivatives of kinetin protect skin cells against UV light.[22] In those studies, effects of substitution of the purine ring or replacement of the furan moiety was explored. Pharmacological activity of kinetin isosteres is subject of two recent US patents. Whereas 10676475[23] deals with effects on alternative pre-RNA splicing, 10167286[24] deals with PINK1 activation in the context of mitoprotection and neuroprotection. Previously, kinetin isosteres were studied as plant hormones.[25–27]

Here, we report an evaluation of effects of replacing the purine moiety of kinetin (**1**) and 2-chlorokinetin (**2**) by other fused heterocycles (Table 1) on biological activities in several assays related to neurodegenerative diseases.

Table 1
Overview of the tested compounds.

No.	C2 Subst.	C6 substituent	Isostere core
1	-H	furfurylamino-	purine
2	-Cl	furfurylamino-	purine
3	-H	furfurylamino-	3*H*-imidazo[4,5-*b*]pyridine, 1-deazapurine
4	-Cl	furfurylamino-	3*H*-imidazo[4,5-*b*]pyridine, 1-deazapurine
5	-H	furfurylamino-	1*H*-imidazo[4,5-*c*]pyridine, 3-deazapurine
6	-Cl	furfurylamino-	1*H*-imidazo[4,5-*c*]pyridine, 3-deazapurine
7	-H	furfurylamino-	7*H*-pyrrolo[2,3-*d*]pyrimidine, 7-deazapurine
8	-Cl	furfurylamino-	7*H*-pyrrolo[2,3-*d*]pyrimidine 7-deazapurine
9	-H	furfurylamino-	5*H*-pyrrolo[3,2-*d*]pyrimidine, 9-deazapurine
10	-Cl	furfurylamino-	5*H*-pyrrolo[3,2-*d*]pyrimidine, 9-deazapurine
11	-H	furfurylamino-	3*H*-[1,2,3]triazolo[4,5-*d*] pyrimidine, 8-azapurine
12	-H	furfurylamino-	pyrazolo[1,5-*a*]pyrimidine
13	-H	furfurylamino-	pyrazolo[4,3-*d*]pyrimidine
14	-H	furfurylamino-	1-methyl-1*H*-pyrazolo[3,4-*d*] pyrimidine
15	-H	5-methylfurfurylamino-	1*H*-pyrazolo[3,4-*d*]pyrimidine
16	-H	(furfuryl)(methyl)amino-	1-methyl-1*H*-pyrazolo[3,4-*d*] pyrimidine
17	-H	(1-(5-methylfuran-2-yl) ethyl)amino-	1-methyl-1*H*-pyrazolo[3,4-*d*] pyrimidine
18	-H	(5-methylfurfuryl)(methyl) amino-	1-methyl-1*H*-pyrazolo[3,4-*d*] pyrimidine
19	-H	furfurylamino-	thieno[2,3-*d*]pyrimidine
20	-H	furfurylamino-	thieno[3,2-*d*]pyrimidine
21	-H	furfurylamino-	furo[2,3-*d*]pyrimidine
22	-H	furfurylamino-	5,6-dimethylfuro[2,3-*d*] pyrimidine
23	-H	furfurylamino-	quinazoline

2. Material and methods

2.1. Synthesis

The test compounds include both commercial compounds, from Olchemim (kinetin – **1**) and Molport (**14**–**23**), and prepared compounds. The synthesis of the latter is described in detail below. An exception is 2-chlorokinetin (**2**) that was provided by Dr. Mik (Palacký University) and its analytical data correspond to the previously published data.[28]

All chemicals and solvents for synthesis were purchased in analytical or HPLC grade quality from available suppliers and used without further purification. For microwave-assisted synthesis steps, reagents were placed in 10 mL closed vessels and subjected to treatment with a Discover SP microwave reactor (CEM Corporation) using dynamic mode and the following settings: stirring – high, power – 200 W, ramp time – 2 min, temperature 120 °C, hold time – 10 min cycles, powermax - on. Solid-phase synthesis was carried out in plastic reaction vessels (syringes, each equipped with a porous disk) using a manually operated synthesizer. All reactions were carried out at ambient temperature (25 °C) unless stated otherwise. The volume of wash solvent was 10 mL per 1 g of resin. For washing, resin slurry was shaken with the fresh solvent for at least 1 min before changing the solvent. Resin-bound intermediates were dried by a stream of nitrogen for prolonged storage and/or quantitative analysis.

For LC/MS analysis a sample of resin (~5 mg) was treated by TFA in DCM, the cleavage cocktail was evaporated by a stream of nitrogen, and cleaved compounds were extracted into 1 mL of MeCN/H2O (1:1). Prior to biological testing all the residual solvents were removed from the samples by careful lyophilization at −110 °C using a ScanVac Coolsafe 110-4 freeze-dryer. Thin layer chromatography (TLC) was performed on Silica gel 60 F254 plates (Merck) and migrating compounds were detected by 254 nm UV light and/or visualized by vanillin staining. Crude products were purified by column chromatography using 40–63 μm Silikagel (VWR). Compounds cleaved from the resin were purified chromatographically using a C18 reverse phase column (YMC Pack ODS-A, 20 × 100 mm, 5 μm particles), and mobile phase consisting of a gradient formed from 10 mM aqueous ammonium acetate and MeCN, with a flow rate of 15 mL/min.

The LC-MS analyses were performed following published protocols[29] and compounds synthesized on solid phase were analysed using a UHPLC-MS system consisting of an Acquity UHPLC chromatograph, coupled to a single quadrupole mass spectrometer (Waters), and equipped with a photodiode array detector and X-Select C18 column

maintained at 30 °C. The mobile liquid chromatography phase consisted of a linear gradient of 20–80% MeCN balanced with 0.01 M ammonium acetate in H2O, over 2.5 min, followed by a hold at 80% MeCN for 1.5 min and re-equilibration with 20% B for 1 min (flow rate: 600 μL/min). The ESI I source of the MS was operated at discharge current of 5 μA, vaporizer temperature of 350 °C, and capillary temperature of 200 °C.

Melting points of synthesized compounds reported here were determined using a Kofler, Stuart SMP30 or Stuart SMP 40 melting point apparatus and are uncorrected. The elemental analysis of prepared compounds was performed on CHN-O Analyzer EA Flash 1112 Series (Thermo Finnigan). Analyses indicated by the symbols of the elements were within ±0.4% of the theoretical values

NMR spectra were recorded on Bruker Avance (300 or 500 MHz), Jeol ECA-500 MHz, and Jeol ECX500 spectrometers operating at 300 MHz (^{1}H), 75 MHz (^{13}C) or 500 MHz (^{1}H), and 125 MHz (^{13}C), frequencies, respectively. Samples were dissolved in DMSO-d_6 or CDCl3 and the chemical shifts (δ) reported in ppm were calibrated against a residual solvent peak (2.49 ppm for proton - DMSO-d_5, 7.26 ppm for proton – CHCl3) and DMSO-d_6 (39.5 ppm for carbon) or CDCl3 (77.0 ppm for carbon). The NMR spectra are available as Appendix A. Prepared compounds were subjected to HRMS analysis using Agilent 6224 Accurate-Mass TOF LC-MS with dual electrospray/chemical ionization mode with mass accuracy greater than 2 ppm or Dionex Ultimate 3000 chromatograph and Exactive Plus Orbitrap Elite high-resolution mass spectrometer (ThermoFisher, MA, USA) operating in positive full scan mode (120 000 FWMH) in the range of 100–1000 *m/z* The oven temperature and source voltage for electrospray ionization were set at 150 °C and 3.6 kV, respectively. The acquired data were internally calibrated with phthalate as a contaminant in MeOH (*m/z* 297.15909). Samples were diluted to a final concentration of 0.1 mg/mL in H2O and MeOH (50:50, v/v). Before HPLC separation (using a Phenomenex Gemini, 50 × 2.00 mm, 3 μm particles, C18 column), the samples were injected by direct infusion into the LC-MS system using an autosampler. The mobile phase was isocratic MeCN/*i*PrOH/0.01 M ammonium acetate (40:5:55) with a flow rate of 0.3 mL/min.

*2.1.1. Synthesis of 3H-imidazo[4,5-b]pyridine (1-deazapurine) derivatives (**I-VII, 3, 4**)*

*2.1.1.1. N-(furan-2-ylmethyl)-3H-imidazo[4,5-b]pyridin-7-amine **(3)**.* Aminomethyl resin (1 g, 0.098 mmol/g) was washed 3× with DCM and 3× with DMF then 10% TEA in DMF (10 mL) was added. After shaking 10 min at rt, the resin was washed 5× with DMF and 4-(4-formyl-3,5-dimethoxyphenoxy)butanoic acid (524 mg), HOBt (229 mg) and DIC (300 mL) in DMF/DCM (1:1, 10 mL) were added. The resin was shaken for 16 h at rt, then washed 3× with DMF, 3× with DCM, 3× with anhydrous THF and 3× with anhydrous DMF. Furfurylamine (442 μL) was dissolved in 10% AcOH/anhydrous DMF (10 mL), the mixture was added to the resin and it was shaken for 16 h at rt. NaBH(OAc)3 (600 mg) was dissolved in 5% AcOH/anhydrous DMF (5 mL), and three equal portions of the solution were added at 1 h intervals to the reaction mixture. After the last addition, the resin was shaken for 16 h at rt, washed 5× with DMF, then shaken with 20% piperidine in DMF (10 mL) for 10 min at rt and washed 5× with DMF and 5× with DCM to obtain the resin **I**. The resin **I** (500 mg) was washed 3× with DMSO and shaken with a solution of 4,6-dichloro-3-nitropyridin-2-amine or 2,4-dichloro-3-nitropyridine (1.54 mmol) and EDIPA (436 μL) in DMSO (5 mL) for 16 h at rt. The resulting resins were washed 3× with DMF and 3× with DCM to obtain the intermediates **II** or **IV**. Resin **IV** was shaken with a solution of 25% aq·NH3 in DMSO for 16 h at 100 °C (in a sealed vial), washed 3× with DMF and 3× with DCM to obtain the resin **V**. Na2S2O4 (1050 mg), K2CO3 (960 mg) and TBAHS (170 mg) were dissolved in DCM/H2O (10 mL, 1:1), added to resins **III** or **V**, the resins were shaken for 16 h at rt, then washed 10× with MeOH/H2O (1:1), 3× with MeOH/DCM (1:1) and 3× with DCM. The resulting resins **VI**(H) or **VI**(Cl) were washed 5× with DMSO, shaken with triethyl orthoformate/DMSO (5 mL, 1:1) for 16 h at 80 °C and washed 5× with DMSO and 5× with DCM. The resins **VII**(H) or **VII**(Cl) were shaken with TFA/DCM (5 mL, 1:1) for 90 min at rt, then washed 5× with TFA/DCM (1:1). TFA/DCM fractions were collected and evaporated with a stream of nitrogen. The crude products **3** or **4** were dissolved in MeCN (10 mL) and purified with semipreparative HPLC.

White solid, overall yield 20% (calculated from the loading of resin **II**). ^{1}H NMR (500 MHz, DMSO-d_6) δ (ppm): 4.62 (d, J = 6.1 Hz, 2H), 6.31 (d, J = 2.9 Hz, 1H), 6.37 (dd, J = 3.2, 1.8 Hz, 1H), 6.41 (d, J = 5.6 Hz, 1H), 7.08 (t, J = 5.9 Hz, 1H), 7.50–7.61 (m, 1H), 7.88 (d, J = 5.6 Hz, 1H), 8.06 (s, 1H). ^{13}C NMR (125 MHz, DMSO-d_6) δ (ppm): 99.0, 107.1, 110.4, 139.0, 142.1, 144.4, 145.2, 148.5, 152.8. HRMS (ESI-TOF): *m/z* calcd. for C11H10N4O $[M+H]^+$ 215.0927, found 215.0930.

*2.1.1.2. 5-chloro-N-(furan-2-ylmethyl)-3H-imidazo[4,5-b]pyridin-7-amine **(4)**.* White solid, overall yield 25% (calculated from the loading of resin **II**). ^{1}H NMR (500 MHz, DMSO-d_6) δ (ppm): 4.64 (bs, 2H), 6.32 (d, J = 2.9 Hz, 1H), 6.39 (dd, J = 3.2, 1.8 Hz, 1H), 6.42 (s, 1H), 7.27–7.47 (m, 1H), 7.58 (dd, J = 1.8, 0.8 Hz, 1H), 8.09 (s, 1H), 12.71 (bs, 1H). ^{13}C NMR (125 MHz, DMSO-d_6) δ (ppm): 39.1, 97.6, 106.9, 110.2, 139.1, 141.9, 145.5, 146.3, 152.1. HRMS (ESI-TOF): *m/z* calcd. for C11H9ClN4O $[M+H]^+$ 249.0538, found 249.0540.

*2.1.2. Synthesis of 1H-imidazo[4,5-c]pyridine (3-deazapurine) derivatives (VIII-X, **5, 6**)*

Resin **II** (500 mg) was washed 5× with DMSO and shaken with 2-chloro-3-nitropyridin-4-amine or 2,6-dichloro-3-nitropyridin-4-amine (2.5 mmol) with EDIPA (436 μL) in DMSO (5 mL) for 16 h at rt, then washed 3× with DMSO and 3× with DCM. Na2S2O4 (1050 mg), K2CO3 (960 mg) and TBAHS (170 mg) were dissolved in DCM/H2O (10 mL, 1:1) and added to resins **VIII**(H) or **VIII**(Cl). The resins were shaken 16 h at rt, then washed 10× with MeOH/H2O (1:1), 3× with MeOH/DCM (1:1) and 3× with DCM. The resulting resins **IX**(H) or **IX**(Cl) were washed 5× with DMSO, shaken with triethyl orthoformate/DMSO (5 mL, 1:1) for 16 h at 100 °C and washed 5× with DMSO and 5× with DCM. The resins **X**(H) or **X**(Cl) were shaken with TFA/DCM (5 mL, 1:1) 90 min at rt, then washed 5× with TFA/DCM (1:1). TFA/DCM fractions were collected and evaporated with a stream of nitrogen. The crude products **5** or **6** were dissolved in MeCN (10 mL) and purified with semipreparative HPLC.

*2.1.2.1. N-(furan-2-ylmethyl)-1H-imidazo[4,5-c]pyridin-4-amine **(5)**.* White solid, overall yield 21% (calculated from the loading of resin **IV**). ^{1}H NMR (500 MHz, DMSO-d_6) δ (ppm): 4.69 (d, J = 5.9 Hz, 2H), 6.30–6.39 (m, 1H), 6.21 (s, 1H), 6.79 (d, J = 4.9 Hz, 1H), 6.98 (bs, 1H), 7.51 (s, 1H), 7.70 (d, J = 5.8 Hz, 1H), 8.08 (s, 1H), 12.50 (bs, 1H). ^{13}C NMR (125 MHz, DMSO-d_6) δ (ppm): 37.1, 99.2, 106.0, 110.1, 138.9, 139.6, 141.3, 147.6, 153.7. HRMS (ESI-TOF): *m/z* calcd. for C11H10N4O $[M+H]^+$ 215.0927, found 215.0929.

*2.1.2.2. 6-chloro-N-(furan-2-ylmethyl)-1H-imidazo[4,5-c]pyridin-4-amine **(6)**.* White solid, overall yield 28% (calculated from the loading of resin **IV**). ^{1}H NMR (500 MHz, DMSO-d_6) δ (ppm): 4.64 (bs, 2H), 6.25 (d, J = 2.9 Hz, 1H), 6.37 (dd, J = 3.0, 1.9 Hz, 1H), 6.79 (s, 1H), 7.41 (bs, 1H), 7.55 (d, J = 0.9 Hz, 1H), 8.15 (s, 1H). ^{13}C NMR (125 MHz, DMSO-d_6) δ (ppm): 37.1, 96.9, 106.7, 110.4, 124.2, 140.4, 140.7, 140.8, 141.7, 148.9, 153.3. HRMS (ESI-TOF): *m/z* calcd. for C11H9ClN4O $[M+H]^+$ 249.0538, found 249.0539.

*2.1.3. Synthesis of 7H-pyrrolo[2,3-d]pyrimidine (7-deazapurine) derivatives (**7, 8**)*

*2.1.3.1. N-(furan-2-ylmethyl)-7H-pyrrolo[2,3-d]pyrimidin-4-amine **(7)**.* A mixture of 4-chloro-7*H*-pyrrolo[2,3-*d*]pyrimidine (100 mg, 0.65

mmol), furfurylamine (90 μL, 0.98 mmol) and TEA (225 μL, 1.62 mmol) in dry MeOH (2.6 mL) was heated in a Discover SP microwave reactor in abovementioned conditions for four cycles. Solvent was evaporated under reduced pressure, the residue was treated with water (10 mL) and product was extracted by EtOAc (4 × 10 mL). Combined organic layers were washed with brine (10 mL), dried (Na2SO4) and concentrated *in vacuo*. Crude material was purified by silica gel column chromatography using CHCl3/MeOH as a mobile phase with a MeOH gradient. Yellow solid; yield 60%; ESI$^+$-MS *m/z*: 215.4 [M+H]$^+$. ^{1}H NMR (500 MHz, DMSO-d_6) δ (ppm): 4.68 (d, J = 5.8 Hz, 2H), 6.26 (dd, J = 3.2, 0.8 Hz, 1H), 6.37 (dd, J = 3.1, 1.8 Hz, 1H), 6.57 (dd, J = 3.4, 1.8 Hz, 1H), 7.06 (dd, J = 3.2, 2.3 Hz, 1H), 7.55 (dd, J = 1.7, 0.8 Hz, 1H), 7.84 (t, J = 5.7 Hz, 1H), 8.11 (s, 1H), 11.51 (bs, 1H). ^{13}C NMR (125 MHz, DMSO-d_6) δ (ppm): 36.5, 98.6, 102.6, 106.8, 110.4, 121.0, 141.9, 150.2, 151.2, 153.1, 155.6. HRMS (ESI-TOF): *m/z* calcd. for C11H10N4O [M+H]$^+$ 215.0927, found 215.0926.

*2.1.3.2. 2-chloro-N-(furan-2-ylmethyl)-7H-pyrrolo[2,3-d]pyrimidin-4-amine (**8**).* A mixture of 2,4-dichloro-7*H*-pyrrolo[2,3-*d*]pyrimidine (100 mg, 0.53 mmol), furfurylamine (74 μL, 0.8 mmol) and TEA (185 μL, 1.33 mmol) was refluxed in *n*PrOH (2.13 mL) for 4 h. After cooling at 4 °C for 2 h the resulting solid material was filtered, washed with cold *n*PrOH (3 × 1 mL), cold H2O (5 × 1 mL) and dried. Crude material was purified by silica gel column chromatography using CHCl3/MeOH as a mobile phase with a MeOH gradient. Yellow solid; yield 62%; ESI$^+$-MS *m/z* (rel %): 249.4 [^{35}Cl-M+H]$^+$ (100), 251.4 [^{37}Cl-M + H]$^+$ (35). ^{1}H NMR (500 MHz, DMSO-d_6) δ (ppm): 4.63 (d, J = 5.5 Hz, 2H), 6.30 (dd, J = 3.2, 0.8 Hz, 1H), 6.40 (dd, J = 3.4, 1.8 Hz, 1H), 6.58 (dd, J = 3.4, 1.8 Hz, 1H), 7.08 (dd, J = 3.5, 2.3 Hz, 1H), 7.59 (dd, J = 1.8, 0.9 Hz, 1H), 8.32 (t, J = 5.7 Hz, 1H), 11.70 (bs, 1H). ^{13}C NMR (125 MHz, DMSO-d_6) δ (ppm): 36.6, 99.1, 101.2, 107.3, 110.5, 121.6, 142.1, 150.8, 152.2, 152.3, 156.4. HRMS (ESI-TOF): *m/z* calcd. for C11H9ClN4O [M+H]$^+$ 249.0538, found 249.0537.

*2.1.4. Synthesis of 5H-pyrrolo[3,2-d]pyrimidine (9-deazapurine) derivatives (**9**, **10**)*

*2.1.4.1. N-(furan-2-ylmethyl)-5H-pyrrolo[3,2-d]pyrimidin-4-amine (**9**).* Compound **9** was prepared similarly to the 7-deazapurine analogue (see Section 2.1.3.1), except that five reaction cycles were needed. Yellow solid; yield 25%; ESI$^+$-MS *m/z*: 216.4 [M+H]$^+$. ^{1}H NMR (500 MHz, DMSO-d_6) δ (ppm): 4.71 (d, J = 5.5 Hz, 2H), 6.36 (d, J = 3.1 Hz, 2H), 6.41 (dd, J = 3.4, 1.8 Hz, 1H), 7.50 (d, J = 2.8 Hz, 2H), 7.61 (dd, J = 1.8, 0.9 Hz, 1H), 8.20 (s, 1H), 10.97 (bs, 1H). ^{13}C NMR (125 MHz, DMSO-d_6) δ (ppm): 36.5, 101.2, 107.4, 110.6, 113.7, 127.9, 142.4, 146.1, 148.9, 149.8, 152.4. HRMS (ESI-TOF): *m/z* calcd. for C11H10N4O [M+H]$^+$ 215.0927, found 215.0926

*2.1.4.2. 2-chloro-N-(furan-2-ylmethyl)-5H-pyrrolo[3,2-d]pyrimidin-4-amine (**10**).* Compound **10** was prepared similarly to the 7-deazapurine analogue (see Section 2.1.3.2). Pale yellow solid; yield 57%; ESI$^+$-MS *m/z* (rel. %): 249.1 4 [^{35}Cl-M + H]$^+$ (100), 251.0 [^{37}Cl-M + H]$^+$ (31). ^{1}H NMR (500 MHz, DMSO-d_6) δ (ppm): 4.66 (d, J = 4.6 Hz, 2H), 6.32 (d, J = 3.1 Hz, 1H), 6.39 (dd, J = 3.2, 0.8 Hz, 1H), 6.43 (dd, J = 3.1, 1.8 Hz, 1H), 7.53 (d, J = 3.1 Hz, 1H), 7.63 (dd, J = 1.8, 0.9 Hz, 1H), 7.85 (bs, 1H), 11.03 (bs, 1H). ^{13}C NMR (125 MHz, DMSO-d_6) δ (ppm): 36.6, 101.2, 107.8, 110.6, 112.4, 129.3, 142.6, 148.3, 149.9, 150.8, 151.6. HRMS (ESI-TOF): *m/z* calcd. for C11H9ClN4O [M+H]$^+$ 249.0538, found 249.0537.

2.1.5. Synthesis of N-(furan-2-ylmethyl)-3H-[1,2,3]triazolo[4,5-d] pyrimidin-7-amine (XI-XV, 11)

*2.1.5.1. Benzyl azide (**XI**).* Benzyl bromide (17.84 mL, 0.15 mol) was added to a solution of NaN3 (11 g, 0.17 mol) in DMSO (300 mL) and the mixture was stirred in the dark at room temperature for 9 h. The reaction was quenched by adding ice cold water and the product was extracted by Et2O. Combined organic layers were carefully concentrated under reduced pressure to give an oily liquid that was used further without purification. Oily liquid; yield 79%. ^{1}H NMR (300 MHz, CDCl3) δ (ppm): 7.24–7.48 (m, 5H), 4.35 (s, 2H). ^{13}C NMR (125 MHz, CDCl3) δ (ppm): 54.9, 128.4 (2 × C), 128.5, 129.0 (2 × C), 135.5.

*2.1.5.2. 5-amino-1-benzyl-1H-1,2,3-triazole-4-carboxamide (**XII**).* 2-Cyanoacetamide (11.83 g, 0.14 mol) was added to a solution of sodium ethoxide (Na – 3.23 g, 0.14 mol, EtOH – 190 mL) to give a white suspension. Benzyl azide (**XI**) (18.2 g, 0.13 mol) was added and the reaction mixture was heated at 90 °C overnight. The resulting solid was filtered, washed with EtOH, then water and dried. A second portion of product was obtained after concentration of the reaction mixture under reduced pressure and treatment with water. Off-white solid, yield 69%, m.p. 236–237 °C, ESI$^+$-MS *m/z*: 217.8 [M+H]$^+$ (100). ^{1}H NMR (500 MHz, DMSO-d_6) δ (ppm): 5.38 (s, 2H), 7.17. (d, J = 7.3 Hz, 2H), 7.26 (t, J = 7.3 Hz, 1H), 7.32 (t, J = 7.4 Hz, 2H). ^{13}C NMR (125 MHz, DMSO-d_6) δ (ppm) 48.8, 122.2, 127.9 (2 × C), 128.2, 129.1 (2 × C), 136.5, 145.4, 164.8.

*2.1.5.3. 3-Benzyl-3,6-dihydro-7H-[1,2,3]triazolo[4,5-d]pyrimidin-7-one (**XIII**).* Ethyl formate (2.22 mL, 27.6 mmol) was added to a mixture of **XII** (2 g, 9.21 mmol) in sodium ethoxide solution (Na – 1.06 g, 46 mmol, EtOH – 50 mL). The mixture was heated in a pressure tube at 95 °C for 24 h. After cooling the pH of the reaction mixture was adjusted to 6, resulting in formation of solid material. The product was filtered off and recrystallized from ethanol. White solid; yield 84%; m.p. 194–195 °C. ESI$^+$-MS *m/z*: 228.8 [M+H]$^+$. ^{1}H NMR (500 MHz, DMSO-d_6) δ (ppm): 5.70 (s, 2H), 7.24–7.31 (m, 5H), 8.22 (s, 1H), 12.70 (s, 1H). ^{13}C NMR (125 MHz, DMSO-d_6) δ (ppm): 50.3, 128.4 (2 × C), 128.7, 129.3 (2 × C), 130.2, 135.9, 149.1, 150.5, 155.9.

*2.1.5.4. 3-Benzyl-7-chloro-3H-[1,2,3]triazolo[4,5-d]pyrimidine (**XIV**).* A mixture of SOCl2 (10.13 mL, 139.6 mmol) and DMF (1.82 mL) was added to a solution of **XIII** (2.54 g, 11.17 mmol) in CHCl3 (100 mL). The reaction mixture was refluxed for 2 h then evaporated *in vacuo*. The residue was mixed with ice-cold water (30 mL) and the resulting mixture was extracted by Et2O (100 mL). After evaporation of Et2O, crude product was purified by silica column chromatography using petroleum ether/ethyl acetate (9:2, v/v) as a mobile phase. Off-white solid; yield 50%; m.p. 223–239 °C. ESI$^+$-MS *m/z* (rel. %): 246.0 [M+H]$^+$ (100). ^{1}H NMR (500 MHz, CDCl3) δ (ppm): 5.87 (s, 2H), 7.29–7.35 (m, 3H), 7.45 (dd, J = 7.9, 1.5 Hz, 2H), 8.91 (s, 1H). ^{13}C NMR (125 MHz, CDCl3) δ (ppm): 51.5, 128.6 (2 × C), 129.0, 129.2 (2 × C), 133.9, 134.2, 149.8, 154.3, 155.7.

*2.1.5.5. 3-Benzyl-N-(furan-2-ylmethyl)-3H-[1,2,3]triazolo[4,5-d]pyrimidin-7-amine (**XV**).* A mixture of **XIV** (0.2 g, 0.81 mmol), furfurylamine (68 μL, 0.77 mmol) and EDIPA (0.7 mL, 40.7 mmol) in *i*PrOH (8 mL) was heated at 100 °C for 4.5 h. After cooling the product started to precipitate. The solid was filtered, washed with *i*PrOH (10 mL), then water (10 mL) and dried. Pale yellow solid; yield 84%; m.p. 169–170 °C. ESI$^+$-MS *m/z* (rel. %): 306.8 [M+H]$^+$ (100). ^{1}H NMR (500 MHz, CDCl3) δ (ppm): 4.88 (d, J = 5.8 Hz, 2H), 5.75 (s, 2H), 6.32 (s, 2H), 6.80 (s, 1H), 7.27–7.41 (m, 6H), 8.53 (s, 1H). ^{13}C NMR (125 MHz, CDCl3) δ (ppm): 37.6, 50.6, 108.2, 110.6, 124.9, 128.4 (2 × C), 128.6, 129.0 (2 × C), 134.9, 142.7, 148.7, 150.6, 154.4, 157.1.

*2.1.5.6. N-(furan-2-ylmethyl)-3H-[1,2,3]triazolo[4,5-d]pyrimidin-7-amine (**11**).* Sodium (37 mg, 1.63 mmol) was added at −78 °C to liquid ammonia (25 mL) and stirred until complete dissolution. **XVII** (0.1 g, 0.33 mmol) was added and the reaction mixture was stirred at −78 °C for 1 h. After evaporation, the residue was treated with water and the pH

of the mixture adjusted to 5–6, resulting in precipitation of product. The solid was filtered off, washed with water and dried. Off-white solid; yield 62%; m.p. 244–245 °C. ESI$^+$-MS *m/z* (rel. %): 217.1 [M+H]$^+$ (100). ^{1}H NMR (500 MHz, DMSO-d_6) δ (ppm): 4.74 (d, J = 5.8 Hz, 2H), 6.29 (d, J = 3.0 Hz, 1H), 6.37 (d, J = 1.8 Hz, 1H), 7.56 (s, 1H), 8.38 (s, 1H), 9.28 (s, 1H). ^{13}C NMR (125 MHz, DMSO-d_6) δ (ppm): 37.0, 107.7, 111.0, 123.9, 142.6, 143.0, 152.4, 154.4, 156.7. HRMS (ESI-TOF): *m/z* calcd. for C9H8N6O [M+H]$^+$ 217.0838, found 249.0845.

2.1.6. Synthesis of N-(furan-2-ylmethyl)pyrazolo[1,5-a]pyrimidin-7-amine (12)

Furfurylamine (180 μL, 1.95 mmol) and K2CO3 (360 mg, 2.60 mmol) were added to a solution of 7-chloropyrazolo[1,5-*a*]pyrimidine (200 mg, 1.30 mmol) in anhydrous acetonitrile (8 mL) and DMF (2 mL) and the reaction mixture was stirred at 90 °C for 3 h. The solvents were evaporated under reduced pressure, the residue was mixed with H2O (30 mL), and the mixture was extracted with EtOAc (2 × 50 mL). Combined organic extracts were washed with brine (50 mL), dried over MgSO4 and concentrated under reduced pressure. The residue was purified by silica gel flash column chromatography using DCM/EtOAc (3:2) as a mobile phase. White solid; yield 34%; m.p. 120–122 °C. ^{1}H NMR (500 MHz, CDCl3) δ (ppm): 4.59 (d, J = 5.8 Hz, 2H), 6.06 (d, J = 5.2 Hz, 1H), 6.32–6.38 (m, 2H), 6.53 (d, J = 2.3 Hz, 1H), 6.84 (s, 1H), 7.35–7.45 (m, 1H), 8.00 (d, J = 2.3 Hz, 1H), 8.25 (d, J = 5.2 Hz, 1H). ^{13}C NMR (125 MHz, CDCl3) δ (ppm): 39.4, 85.3, 95.9, 108.6, 110.7, 143.0, 143.9, 146.9, 149.6, 149.7. HRMS (APCI): *m/z* calc. for C11H11N4O [M+H]$^+$ 215.0927, found 215.0925.

2.1.7. Synthesis of 1H-pyrazolo[4,3-d]pyrimidine derivative (XVI, XVII, 13)

2.1.7.1. 1H-pyrazolo[4,3-d]pyrimidine-7-thiol (XVI). 1*H*-pyrazolo[4,3-*d*]pyrimidine-7-thiol was prepared from 1*H*-pyrazolo[4,3-*d*]pyrimidin-7-ol according to the published procedure.[30]

2.1.7.2. 7-(methylthio)-1H-pyrazolo[4,3-d]pyrimidine (XVII). A solution of MeI (144 mg, 1 mmol) in DMF (2.8 mL) was added dropwise at 0 °C to a mixture of **XVI** (153 mg, 1 mmol) and K2CO3 (152 mg, 1.1 mmol) in DMF (7.5 mL). The reaction mixture was allowed to warm to rt then stirred for an additional 10 min. After evaporation *in vacuo* the residue was partitioned between H2O and DCM. The product was finally obtained by crystallization from DCM. White solid; yield 84%; m.p. 195–200 °C; UV (nm): max. 308, sh 319. ESI$^-$-MS (*m/z*): 165.1 [M−H]$^-$.

2.1.7.3. N-(furan-2-ylmethyl)-1H-pyrazolo[4,3-d]pyrimidin-7-amine (13). A mixture of **XVII** (93 mg, 0.56 mmol) in furfurylamine (3 mL) was heated at 125 °C for 8 h. After evaporation under reduced pressure the crude material was purified by silica gel column chromatography using stepwise increments of MeOH (3, 4, and 5%) in CHCl3. Product was finally obtained by crystallization from CHCl3. White solid; yield 66%, m.p. 182–185 °C; UV λ (nm): min. 253, max. 292, sh 305. ESI$^+$-MS (*m/z*): 216.1 [M+H]$^+$, ESI$^-$-MS (*m/z*): 214.1 [M+H]$^+$. ^{1}H NMR (500 MHz, DMSO-d_6) δ (ppm): 4.75 (bs, 2H), 6.38 (s, 1H), 6.41 (s, 1H), 7.61 (s, 1H), 7.93 (bs, 1H), 8.12 (s, 1H), 8.26 (s, 1H), 12.72 (bs, 1H). ^{13}C NMR (125 MHz, DMSO-d_6) δ (ppm): 36.4, 107.6, 110.5, 121.0, 133.1, 141.4, 142.4, 148.7, 151.7. Anal. (C10H9N5O) C,H,N.

2.2. Fibroblast cell culture

Skin fibroblasts GM04078 homozygous for the GAA expansion in the frataxin gene and skin fibroblast GM04663, which are homozygous for the 2507 + 6 T > C mutation in the ELP1 gene, were obtained from the Coriell repository. The cells were maintained in Dulbecco's modified Eagle's medium (DMEM) containing 5 g/L glucose, 2 mM L-glutamine, 100 U/mL penicillin, 100 μg/mL streptomycin and 10% fetal bovine serum (FBS) (Sigma) in standard culture conditions (5.5% CO2, 37 °C, 100% relative humidity). The cells were subcultured twice a week.

2.3. Fibroblast culture stress assays

GM04078 fibroblasts were trypsinized, diluted in DMEM medium with 10% FBS and seeded into 384-well plates (1500 cells in 30 μL medium/well). After 24 h incubation, the cells were pre-treated by the test compounds dissolved in DMSO using an Echo 555 system (Labcyte). DMSO vehicle served as a negative control. Stressors were added in 15 μL of the medium used for seeding after 8 h. After another 48 h, 15 μL of a 4-fold concentrated solution of resazurin (Sigma) in the culture medium was added to the cells to a final concentration of 0.0125 mg/mL. Fluorescence was measured after 3 h incubation using an M2 reader (Biotek) with excitation and emission wavelengths of 570 and 610 nm, respectively.

2.4. Reduced glutathione measurements

GM04078 fibroblasts were trypsinized, diluted in DMEM medium with 10% FBS and seeded into 384-well plates (1500 cells in 30 μL medium/well). After 24 h incubation, the cells were pre-treated by adding compound **6** dissolved in DMSO (final concentration 10 and 50 μM) using the Echo 555 system. DMSO vehicle served as a negative control. BSO was added (to serial concentrations of 10, 100 and 1000 μM) in 15 μL portions of medium after 8 h. The effect was evaluated after 24 h, when the medium was removed and, after a washing with 100 μL DMEM medium, replaced by DMEM medium containing 40 μM monobromobimane. After 40 min incubation, images were recorded, at 4× magnification using the blue channel of a Cell Voyager confocal imaging system. The intensity of the signal was evaluated by an image analysis tool in the Cell Profiler program. Control measurement using spectrophotometer (ex 395 nm, em 490 nm) was also performed.

2.5. Frataxin assay

To test the ability of compounds to replace frataxin (FXN) functionally, enzymatic assays were performed using mouse ISC machinery reconstituted *in vitro* with purified proteins [31]. The assays were performed under anaerobic conditions in Tris buffer (50 mM Tris, 150 mM NaCl, pH 8) containing 50 μM of apo-ISCU loaded with one equivalent of Fe^{2+}, 5 μM of the NFS1-ISD11-ACP complex, 5 μM of FDX2, 2 μM of FDXR and 100 μM of NADPH. Positive controls were prepared by adding 5 μM of FXN to the reaction mixture. Test compounds diluted in DMSO were added to the reaction mixture at concentrations of 30, 50, 100, 200 and 500 μM and supplementary DMSO was added to the reaction mixtures to keep its concentration the same in each reaction. Reference reaction mixtures were prepared with the same concentration of DMSO as the mixtures with test compounds. The reactions were initiated by adding 50 μM of L-cysteine and the formation of Fe-S clusters was monitored by UV–visible spectroscopy at 456 nm and 30 °C. Rates of the reactions were determined by linear regression of the slopes of the resulting curves in their linear domain between 2 and 10 min, using GraphPad Prism. The compounds' activities were calculated by dividing slopes of their reaction curves by those of the corresponding reference reactions, which yielded activation factors. Activation factors higher and lower than 1 indicate active and inactive compounds, respectively.

2.6. SH-SY5Y cultivation and differentiation

The SH-SY5Y human neuroblastoma cell line obtained from ATCC (American Type Culture Collection, Manassas, VA, USA) was cultivated in DMEM medium and Ham's F12 Nutrient Mixture (DMEM:F-12, 1:1), supplemented with 10% FBS and 1% of both penicillin and streptomycin at 37 °C in a humidified atmosphere of 5% CO2. Only the cells passaged less than 20 times were used in the experiments. The cells were seeded in

96-multiwell plates, in 100 μL total volume of medium per well. Next day, 10 μM of ATRA in DMEM/F12 medium with 1% FBS was added to each well to a final concentration 10 μM to induce neuronal differentiation. The cells were used for experiments 48 h later. The same protocol was used for the SH-SY5Y obtained from ECACC (European Collection of Authenticated Cell Culture).

2.7. Evaluation of compounds' cytoprotective activity toward differentiated SH-SY5Y cells

Portions of culture containing 20,000 SH-SY5Y cells were seeded into 96-well plates and differentiated by ATRA as outlined above. The differentiation medium was removed and replaced by fresh DMEM/F12 medium with 1% FBS containing test compounds at 0.1, 1 or 10 μM concentration. DMSO vehicle was used as a negative control. The differentiated cells were immediately exposed to glutamate (160 mM), and the frequency of dead cells was assessed using propidium iodide (PI) as a probe after another 24 h, following the published protocol[32] with modification. Briefly, PI (Sigma Aldrich) was diluted to 1 mg/mL in DMSO. This solution was further diluted in PBS then added to the cells' medium to a final concentration of 1 μg/mL, then the cells were incubated at rt for 15 min. Proportions of PI-stained cells were quantified using an Infinite M200 Pro reader (Tecan) with 535 excitation and emission wavelengths of 535 and 617 nm, respectively.

2.8. Measurement of caspase 3/7 activity

To assess the effects of test compounds on glutamate-induced apoptosis, SH-SY5Y cells were subjected to the differentiation and treatment steps described in the previous section, and then to the one-step caspase 3/7 assay described by Carrasco et al. in 2003[33] with modification of the caspase-3,7 substrate concentration, which was decreased to 75 μM. Caspase-3,7 activity was quantified using an Infinite M200 Pro (Tecan, Austria) microplate reader with excitation and emission wavelengths of 346 and 438 nm, respectively after 3-hour incubation. The average signal of the samples treated with glutamate corresponds to 100% caspase 3/7 activity.

2.9. Measurement of oxidative stress

To assess the effects of test compounds on glutamate-induced oxidative stress, SH-SY5Y cells were subjected to the differentiation and treatment steps described in the Section 3.5, and then the dihydroethidium assay described by Kim et al. in 2017[34] with the following modifications. After 4 h of exposure to glutamate, cells were centrifuged at 500 g for 330 s with subsequent replacement of media by PBS containing 10 μM dihydroethidium (DHE). Finally, plates with cells were kept at rt for 30 min, then superoxide radical formation (DHE) signal was quantified using an Infinite M200 Pro reader (Tecan) with excitation and emission wavelengths of 500 and 580 nm, respectively.

2.10. Evaluation of compounds' effects on alternative splicing of ELP1 transcripts

GM04663 cells in DMEM medium with 10% FBS were seeded in 10 cm Petri dishes (about 500,000 cells per dish) and grown overnight before treatment with the test compounds at 50 μM concentration to test their effects on alternative splicing of ELP1 transcripts. Kinetin (compound **1**) and 2-chlorokinetin (compound **2**) were used as positive controls. DMSO vehicle served as a negative control. After 24 h, total RNA was extracted from the cells using Trizol reagent. Isolated RNA was transcribed into cDNA using a High Capacity cDNA Reverse Transcription Kit (Applied Biosystems). The ELP1 cDNA segment between nucleotides 2194 and 2593 (numbering corresponding to the NM_003640.5 transcript) was amplified by the polymerase chain reaction using 5′-CAGGTGTCGCTTTTTCATCA-3′ and 5′-CATTTCCAAGAAACACCTTAGGG-3′ primers[35] and JumpStart *Taq* DNA Polymerase with MgCl2 (Sigma-Aldrich). The temperature program involved: initial denaturation at 94 °C for 5 min followed by 34 cycles of denaturation at 94 °C for 40 s, annealing at 63.8 °C for 30 s and elongation at 72 °C for 90 s, with a final elongation step at 72 °C for 5 min. The PCR products corresponding to wild-type ELP1 transcript (422 bp) and transcript lacking exon 20 (348 bp) were separated by electrophoresis in 1.5% agarose gel and visualized by GelRed staining. For final comparison of the compounds identified as active during the initial screening, microfluidic electrophoresis (with an Agilent 2100 Bioanalyzer and 1000 LabChip kit) was used. A comparison with DNA standards of known size and concentration allowed precise quantification of the wild-type and aberrant transcripts' concentrations. The area under the peak calculations were carried out in the 2100 Expert Software.

2.11. Western blotting and immunodetection of frataxin

For this purpose, GM4078 cells in DMEM medium with 10% FBS were seeded in 10 cm Petri dishes (about 1.4 million cells per dish) and 24 h later treated with 10 and 50 μM of compound **6.** The cells were harvested after 48 h. Medium was removed and the cell monolayer was washed twice with ice-cold PBS. The cells were scraped into 2 mL ice-cold PBS and centrifuged. The supernatant was removed and each pellet was flash-frozen by dipping the tube into liquid nitrogen. The samples were stored at −80 °C.

Total protein was extracted by direct cell lysis in Laemmli buffer (50 mM Tris-HCl, pH 6.8, 2% SDS, 10% glycerol, 0.04% bromophenol blue, and 250 mM mercaptoethanol). The protein concentrations in the samples were determined by Bradford's method and standardized. The samples were boiled for 10 min and stored at −20 °C.

The protein lysates (25–40 μg) were separated by SDS-PAGE (12.5% gel). Proteins were transferred to polyvinylidene difluoride membrane (Bio-Rad) pre-treated by incubation in a 5% solution of bovine serum albumin (BSA) with 1x PBS-Tween (PBS-T) for 2 h. The membrane was then incubated with anti-frataxin mouse antibody (18A5DB1 Abcam) in BSA for 2 h in PBS-T, followed by three washes with PBS-T. For loading standardization, a portion of the membrane was incubated with anti-actin antibody. The membrane was then incubated with a secondary (horseradish peroxidase-conjugated anti-mouse) antibody for 60 min followed by three washes with PBS-T. The immunoblots were then developed using Amersham ECL reagents.

2.12. In vitro permeability assays

Parallel artificial membrane permeability, chemical stability, stability in human plasma, microsomal stability and protein plasma binding assays were performed using methods described by Borková et al. In 2019.[36]

2.12.1. Quantification of test compounds in the permeability assays

Preparation of lyophilized samples for this analysis is described in the sections dedicated to the *in vitro* ADME assays. Test compounds in the samples were quantified using a RapidFire RF300 system (Agilent Technologies) interfaced with a QTRAP 5500 mass spectrometer fitted with an electrospray ionization source (AB Sciex, Concord, Canada) running in multiple-reaction monitoring mode.

Lyophilized samples were dissolved in the mobile phase (95% water, 5% acetonitrile, 0.1% formic acid) with respective internal standards. The dissolved samples were aspired directly from 96-well plates into a 10 μL sample loop and passed through a C4 cartridge (Agilent Technologies) with solvent A (95% water, 0.01% formic acid, 5% acetonitrile) at a flow rate of 1.5 mL/minute for 3 s. After the desalting step, the analyte retained on the cartridge was eluted with solvent B (95% acetonitrile, 5% 0.01% formic acid) into the mass spectrometer at a flow rate of 0.4 mL/minute for 7 s, where it was subjected to electrospray

ionization in the positive ion mode and daughter ion was identified.

2.12.2. Studies of transport across Caco-2 and MDCK-MDR1 cell monolayers

To generate cell monolayers for transport studies,[37,38] the cells were trypsinized and seeded on tissue culture polyester membrane filters with pore size 1 μm in 96-well Transwell® plates (Corning, NY, USA). Culture medium was added to both the donor and the acceptor compartments and the cells were allowed to differentiate and form monolayers. The culture medium was changed every other day.

MDR1-MCDK differentiated monolayers were used only if they were intact, as confirmed by the Lucifer Yellow Rejection Assay. Before each experiment, the cells were washed twice with Hank's balanced buffer solution (HBBS) (Gibco, Waltham, USA) and pre-equilibrated with HBSS buffered at pH 7.4 for 1 h. After removing the medium, MDCK-MDR1 cells were treated with test compounds at 10 μM in HBSS (pH 7.4) for 1 h, then samples were removed from both donor and acceptor compartments and lyophilized. All experiments were done in duplicates.

Apparent permeability coefficients were calculated as Papp = (dQ/dt)/(C0 × A), where dQ/dt is the rate of permeation of the test compound across the cell monolayer, C0 is the donor compartment concentration at time t = 0 and A is the area of the cell monolayer. The efflux ratio R was defined as the ratio PBA/PAB where PBA and /PAB are the apparent permeability coefficients of the test compound from the basal to apical and apical to basal sides of the cell monolayer, respectively. Compounds with an efflux ratio of ≥ 2 were considered potential P-gp substrates.

2.13. Data analysis

Statistical significance of the compound effect was evaluated by non-parametric Kruskal-Wallis test followed by post-hoc Man-Whitney test and sequential Bonferroni correction using the GrahpPad and PAST (ver. 1.97)[39] software packages. Differences with the corrected p-values < 0.05 were considered statistically significant. The error bars in graphs are standard errors, unless stated otherwise. Standard errors for drug efflux ratios were calculated by the Delta method described in[40] implemented in R.

3. Results and discussion

A series of kinetin (**1**) and 2-chlorokinetin (**2**) purine bioisosteres were prepared (Figs. 1, 2) and screened for their biological activity. Although the majority of the compounds is known in either peer reviewed literature or patents, synthesis and characterization was reported only for compounds **3**, **5, 7** and **11**. Moreover, with exception of compound **7**, we used different synthetic routes as described below. We also evaluated biological effects of commercially available derivatives. Those included 1*H*-pyrazolo[3,4-*d*]pyrimidine analogues methylated on the *N*1 nitrogen atom and/or furfurylamino moiety (**14**–**18**) as well as thieno[2,3-*d*]pyrimidine (**19**), thieno[3,2-*d*]pyrimidine (**20**), furo[2,3-*d*]pyrimidine (**21**, **22**), and quinazoline (**23**) (Fig. 3).

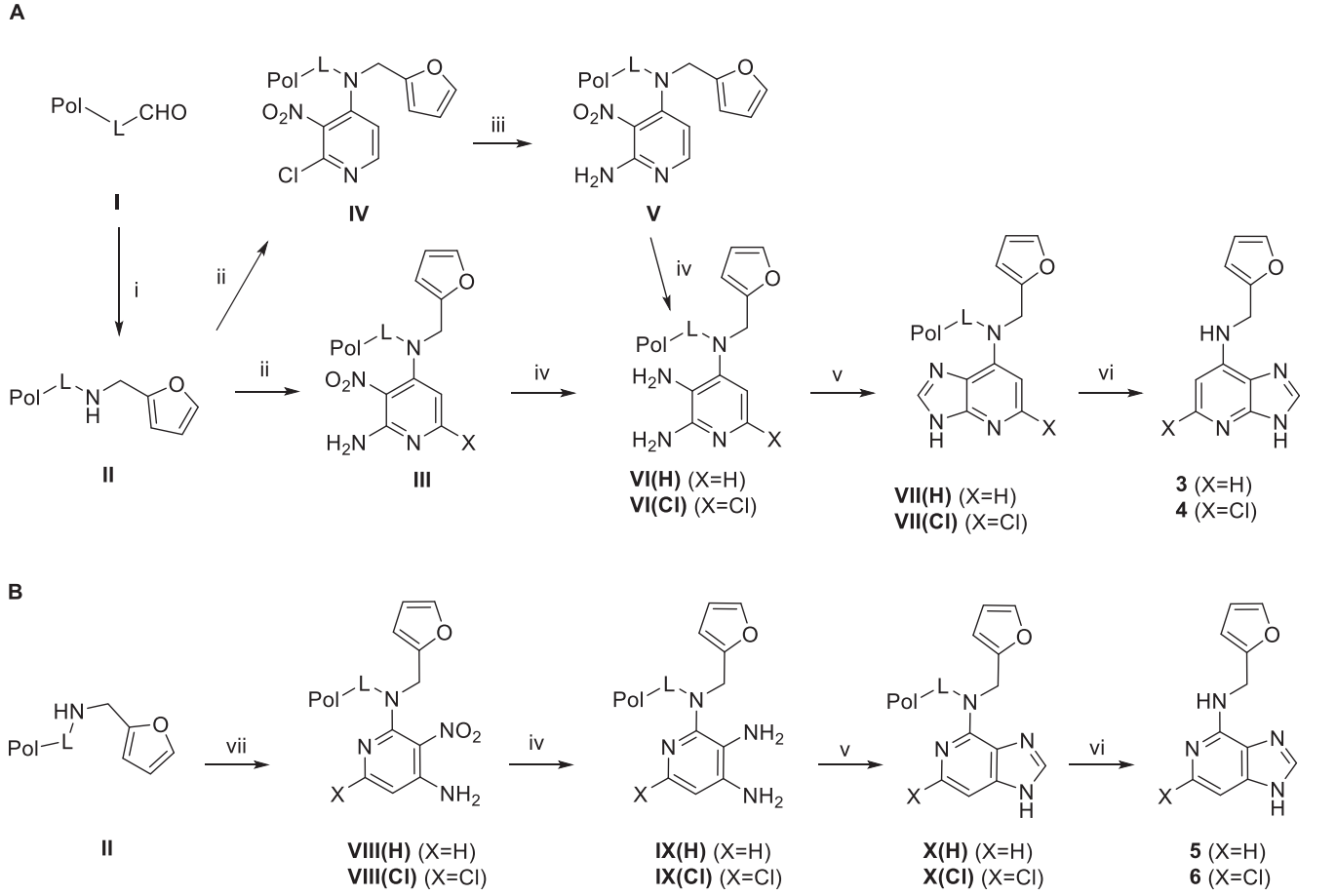

Fig. 1. Synthesis of 2-H and 2-Cl imidazo[4,5-*b*]pyridines (1-deazapurine, scheme A) and imidazo[4,5-*c*]pyridines (3-deazapurine, scheme B) kinetin isosteres. Reagents and conditions: (i) (a) furfurylamine, 10% AcOH in anh. DMF, 16 h, rt; (b) $NaBH(OAc)_3$, 5% AcOH in anh. DMF, 16 h, rt; (ii) 4,6-dichloro-3-nitropyridin-2-amine or 2,4-dichloro-3-nitropyridine, EDIPA, DMSO, 16 h, rt; (iii) DMSO, 25% aq·NH_3, 16 h, 100 °C; (iv) $Na_2S_2O_4$, K_2CO_3, TBAHS, DCM/H_2O, 16 h, rt; (v) triethyl orthoformate/DMSO (1:1), 16 h, 80 °C; (vi) TFA/DCM (1:1), 90 min, rt; (vii) 2-chloro-3-nitropyridin-4-amine or 2,6-dichloro-3-nitropyridin-4-amine, EDIPA, DMSO, 16 h, rt.

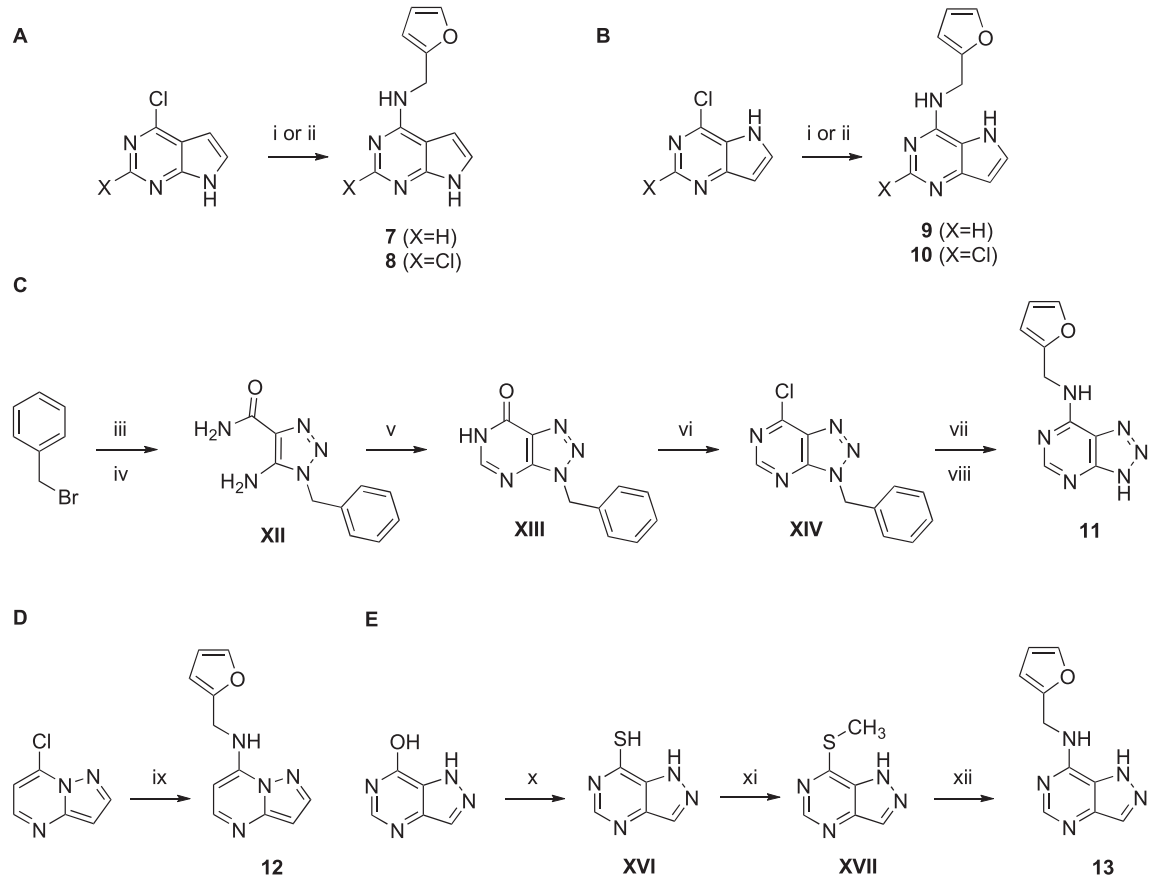

Fig 2. Synthesis of 2-H and 2-Cl pyrrolo[2,3-*d*]pyrimidines (7-dezapurines, scheme A), pyrrolo[3,2-*d*]pyrimidines (9-deazapurines, scheme B), triazolo[4,5-*d*]pyrimidine (8-azapurine, scheme C), pyrazolo[1,5-*a*]pyrimidine (scheme D), and pyrazolo[4,3-*d*]pyrimidine (scheme E) kinetin isosteres. Reagents and conditions: (i) furfurylamine, TEA, 120–170 °C, MW irradiation, 40–50 min; (ii) furfurylamine, TEA, *n*PrOH, reflux, 4 h; (iii) NaN_3, DMSO, rt (XI); (iv) 2-cyanoacetamide, EtONa, EtOH, 90 °C; (v) ethyl formate, EtONa, EtOH, 95 °C; (vi) $SOCl_2$, DMF/$CHCl_3$, reflux; vii) furfurylamine, EDIPA, iPrOH, 100 °C, 4.5 h (XV); (viii) Na, NH_3, −78 °C, 1 h; (ix) furfurylamine, K_2CO_3, MeCN/DMF, 90 °C, 3 h; (x) P_2S_5, Py, reflux 3 h; (xi) MeI, K_2CO_3, DMF, 0 °C to rt, 10 min; (xii) furfurylamine, 125 °C, 8 h.

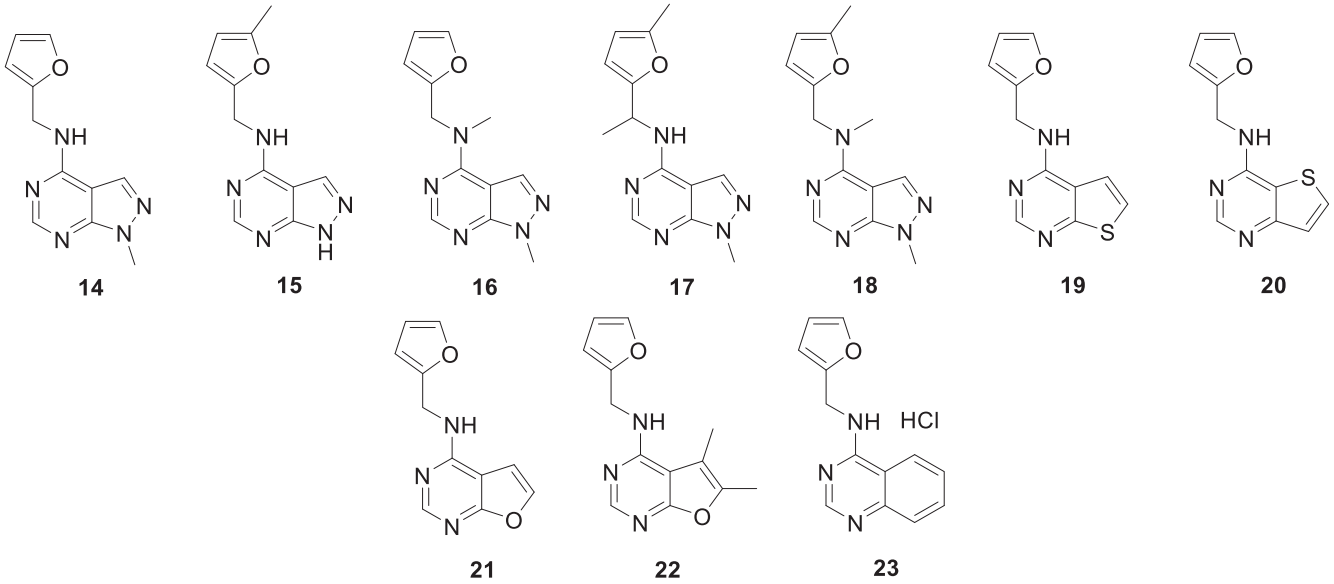

Fig. 3. Structures of commercially available kinetin isosteres.

3.1. Chemistry

Imidazo[4,5-*b*]pyridines (**3**, **4**) and imidazo[4,5-*c*]pyridines (**5**, **6**) were synthesized similarly to previously reported procedures[41,42] using solid-phase synthesis (Fig. 1). Aminomethyl resin with acid-labile benzaldehyde linker **I** was reductively aminated with furfurylamine to give the resin **II**. To synthesize the chlorinated imidazo[4,5-*b*]pyridine **VII(Cl)**, the resin **II** was arylated with 4,6-dichloro-3-nitropyridin-2-

amine and intermediate **III** was obtained. After reduction with sodium dithionite, the resulting resin-bound intermediate **VI(Cl)** was cyclized with triethyl orthoformate, which afforded the polymer-supported imidazo[4,5-*b*]pyridine **VII(Cl)**. Final cleavage using trifluoroacetic acid yielded the desired product **4** (Fig. 1A).

The corresponding unsubstituted imidazo[4,5-*b*]pyridine **3** was prepared analogically using 2,4-dichloro-3-nitropyridine in the arylation step. The resin **IV** was subjected to amination with a mixture of aqueous ammonia and dimethylsulfoxide (DMSO) to obtain the resin **V** followed by the reduction and cyclization of the resin-bound intermediate **VI(H)** with triethyl orthoformate. Cleavage from the resin yielded crude imidazo[4,5-*b*]pyridine **3**. Cleaved compounds **3** and **4** were purified using semipreparative reverse-phase chromatography. Imidazo[4,5-*c*]pyridines **5** and **6** were prepared in a similar way using either 2-chloro-3-nitropyridin-4-amine or 2,6-dichloro-3-nitropyridin-4-amine to arylate the resin **II**. The rest of the reaction sequence was identical to preparation of imidazo[4,5-*b*]pyridines **3** and **4** (Fig. 1B). An alternative synthesis of compounds **3** and **5** using the substitution of the complete purine isostere ring with furfurylamine was reported.[27]

Unsubstituted pyrrolo[2,3-*d*]pyrimidine **7** and pyrrolo[3,2-*d*]pyrimidine **9** isosteres were prepared by microwave-assisted synthesis. A mixture of 4-chloro-7*H*-pyrrolo[2,3-*d*]pyrimidine or 4-chloro-5*H*-pyrrolo[3,2-*d*]pyrimidine with furfurylamine and triethylamine in methanol was subjected to focused microwave irradiation (MW) using a Discover SP reactor (Fig. 2A, B). Similar synthesis of compound **7** was reported by Davoll in 1960[25] but our protocol using MW provided much higher yields (60% vs. 26.2%)0.2-Cl Analogues (**8**, **10**) were prepared by conventionally heating starting material with furfurylamine, and triethylamine in refluxing *n*-propanol (Fig. 2A and B, respectively).

Synthesis of 8-azakinetin (**11**) was started by azidation of benzyl bromide with sodium azide in anhydrous DMSO to give **XI**, followed by cyclization of the triazole ring of **XII** with 2-cyanoacetamide. Pyrimidine ring closure was accomplished with ethyl formate and intermediate **XIII** was subsequently chlorinated by thionyl chloride to obtain compound **XIV**. Substitution of the chlorine atom with furfurylamine yielded compound **XV**. Final debenzylation was achieved by treating **XV** with sodium in liquid ammonia (Fig 2C). Pyrazolo[1,5-*a*]pyrimidine kinetin analogue (**12**) was prepared in just one step by reacting 7-chloropyrazolo[1,5-*a*]pyrimidine with furfurylamine (Fig. 2D), whereas synthesis of compound **13** required a three-step procedure. First, the hydroxy group of 1*H*-pyrazolo[4,3-*d*]pyrimidin-7-ol was converted to thiol by heating the starting compound with phosphorous pentasulfide according to a published protocol,[30] followed by methylation of **XVI** with methyl iodide. Finally, substitution of the methylsulfanyl group of **XVII** with furfurylamine furnished compound **13** (Fig. 2E). An alternative synthesis of compound **11** from 4-amino-6-chloro-5-nitropyrimidin was reported previously.[26]

3.2. Protection of fibroblasts derived from Friedreich ataxia patients against oxidative stress

Friedreich ataxia (FA) is a mitochondrial disease affecting the nervous system and heart caused by a homozygotic mutation in the gene encoding frataxin (FXN), a crucial protein for Fe-S cluster assembly. As a consequence, several essential proteins for mitochondrial energy production are affected, as reviewed by Bürk in 2017.[43] The current therapy only eases the symptoms without addressing the pathological changes of mitochondria and cells. Established screening protocols for candidate drugs exploit the increased sensitivity of FA fibroblasts to stress.[44–46] In a recent high-throughput screening campaign aimed at finding potential new treatments for FA based on evaluation of protection against glutathione depletion (Voller et al., in preparation), we identified 2-chloro-3-deazakinetin as a highly active derivative (compound **6** herein). We decided to further search the chemical space of kinetin derivatives for other active compounds using the same protocol. GM04078 FA fibroblasts were pretreated with the test compounds and then exposed to L-buthionine sulfoximine (BSO), an inhibitor of glutathione *de novo* synthesis. The effect on cell viability was evaluated using the resazurin reduction assay.[47] Protective activity was observed not only for compound 6 but also for compound 5, an analogue with no 2-chloro substituent. Neither kinetin nor 2-chlorokinetin was active (data not shown). Follow-up experiments showed that both compounds **5** and **6** have dose-dependent effects (Fig. 4A), but the effect of compound **6** was much stronger. Compound **6** showed some protective activity at 10 or 50 μM against an even higher dose of BSO (Fig. 4B).

The protective effect of the compounds was not mediated by restoring levels of GSH, which were measured by quantifying fluorescent adducts with monobromobimane (not shown). We also addressed the possibility that the effect of compound **6** could be explained by restoration of FXN expression, but treating FA fibroblasts with the compound at 10 and 50 μM had no clear effects as assessed by western blotting and immunodetection (not shown). We also tested whether compounds **5** and **6** could directly replace the primary function of FXN in the stimulation of iron-sulfur cluster (ISC) biosynthesis.[48] To this end, we used functionally relevant reconstituted ISC machinery without frataxin to test effects of these compounds on the rate of Fe-S cluster synthesis.[31] At 200 μM, compound **5** slightly activated Fe-S cluster biosynthesis by a factor of 1.1, which is only about 0.5% of the activation afforded by FXN (see Appendix B – Fig. B.1). Such a small effect is not consistent with the compound's marked protective effect on BSO-treated cells. Moreover, compound **6**, which also protects against BSO toxicity in FA fibroblasts, slightly inhibits rather than stimulates Fe-S cluster synthesis. Therefore, compound **5** or **6** may influence secondary effects of the lack of FXN in FA fibroblasts rather than Fe-S cluster biosynthesis. Yet another mechanism that could potentially explain protective activity in FA models is iron chelation; however compound 6 had no effect in calcein quenching assay[49] (data not shown).

3.3. The effect on oxidative stress injury in SH-SY5Y cells

Observations of the protective activities of compounds 5 and 6 inspired us to test activities of kinetin isosteres in other disease models where glutathione depletion plays a role. The SH-SY5Y neuroblastoma cell line is often used in neuroprotection research, as reviewed by Xicoy et al. in 2017.[50] One of the frequently used stressors in SH-SY5Y studies is glutamate.[51] At high concentrations, it causes massive oxidative stress by inhibiting the cystine/glutamate Xc-antiporter which resulted in GSH depletion and negative regulation of superoxide dismutase (SOD).[51] Resulting phenotypes are complex; features of necroptosis, apoptosis, and ferroptosis may be present.[52] The changes are probably not triggered by glutamate excitotoxicity, as SH-SY5Y cells probably express only one of the NMDA receptor subunits.[53] However, some other mechanisms have been suggested including, for example, Rac-NADPH-oxidase-driven superoxide radical formation.[51]

We exposed SH-SY5Y cells from American Tissue Type Collection (ATTC) to 160 mM glutamate for 24 h – following enhancement of their differentiation and neuronal phenotype by 48 h treatment with 10 μM all-trans retinoic acid (ATRA) - and assessed the effect of kinetin isosteres on the proportion of dead cells by propidium iodide staining. The iron chelator deferoxamine was used as a positive control. Pilot experiments (not shown) allowed us to focus on several candidates for which protective activity was suspected. Significant activity was confirmed for compounds 6, 10 and 22 (Fig 5A). At 10 μM concentration, they reduced death-indicating propidium iodide signals in cells by more than 10%. However, their effect was lower than that of equimolar deferoxamine. We also assessed the possibility that those compounds may reduce oxidative stress, by quantifying superoxide radical production by dihydroethidium staining, and found that all the candidates had a dose-dependent effect (Fig. 5B).

Protective activity of compound **6** against glutamate-induced stress was further validated by testing in a SH-SY5Y cell line from European Collection of Authenticated Cell Culture (ECCAC) with a different

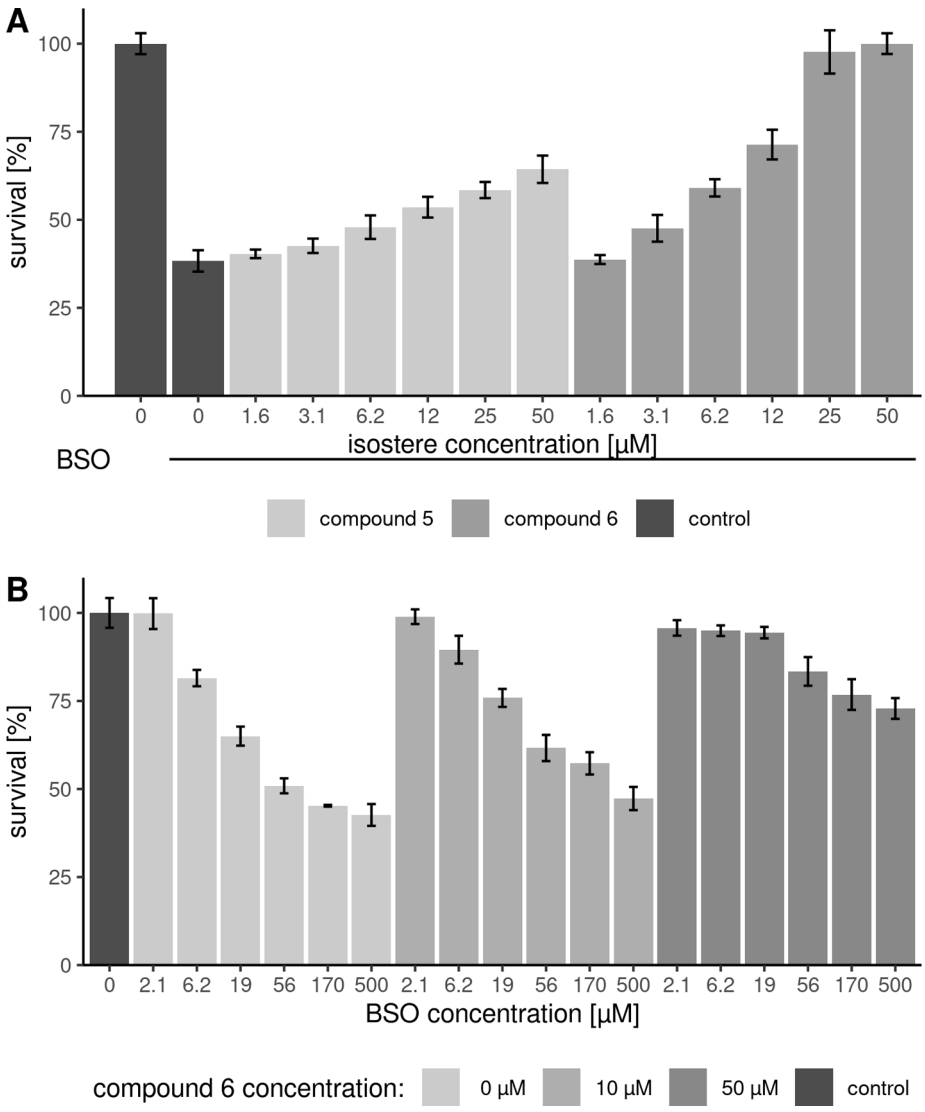

Fig. 4. The protective effect of compounds **5** and **6** against L-buthionine sulfoximine (BSO) in FA-fibroblasts GM04078. Panel A: Pretreatment with serial concentrations of the compounds followed by exposure to 15 μM BSO. Panel B: Pretreatment with compound **6** at 10 or 50 μM followed by exposure to serial concentrations of BSO.

morphology and sensitivity to various toxins.[54] Compound **6** at 10 μM decreased oxidative stress and had a protective activity, albeit the effects were lower than those observed in the cells from ATTC. We also show that the protective effect was partially mediated by inhibition of caspase activation (see Appendix B Fig. B.2). A detailed study of kinetin's behaviour in neuron-like SH-SY5Y will be published separately (González et al., submitted to Molecules journal). Compounds 1-deaza and 3-deazakinetin showed a protective activity in undifferentiated SH-SY5Y against proteotoxic stress induced by MG-132 treatment according to the US patent 20170190704.[24] The effect is supposed to be mediated by PINK1 activation, however no supporting data are shown. As PINK1 activation by kinetin requires its conversion into the corresponding nucleoside monophosphate through the action of adenine phosphoribosyl transferase followed by further enzymatic phosphorylation,[9] the combination of purine ring modification with the presence of 2-chloro substitent suggests that compound **6** and **10** act by a different mechanism.

3.4. Effect of compounds on aberrant splicing of ELP1

We were also interested in the possibility that compound **6** and other derivatives may have beneficial effects in models of neurodegenerative diseases in which kinetin (**1**) or 2-chlorokinetin (**2**) are active. One such disease is familial dysautonomia, a genetic disorder due (as already mentioned) to aberrant splicing of ELP1 transcripts.[20,55] It is known that patient-derived skin fibroblasts can be used for identification of compounds that increase exon 20 inclusion, as in wild-type splicing.

Here, we evaluated the effect of kinetin isosteres at 50 μM on the ratio of wild-type to mutant transcripts in the patient-derived skin fibroblast cell line GM04663. mRNA was reverse-transcribed and ELP1 DNA was amplified by PCR. During the screening phase of the study, the effect of the compounds was evaluated using standard agarose electrophoresis and GelRed staining (not shown). The activity of the hits was then validated by capillary electrophoresis (Fig. 6, Appendix B Fig. B.3).

The results demonstrate that replacement in either the pyrimidine or imidazole rings of the purine moiety can yield active compounds. However, some purine ring modifications led to loss of activity. 1-deaza derivatives of both kinetin and 2-chlorokinetin were active, but not their 3-deaza counterparts, suggesting that the *N3* nitrogen is crucial for the interaction with an unknown molecular target. The activity was retained if either *N7* (compounds **7** and **8**) or *N*9-nitrogen (compounds **9** and **10**) were replaced by a carbon atom. The activity of 1-deaza, 7-deaza and 9-

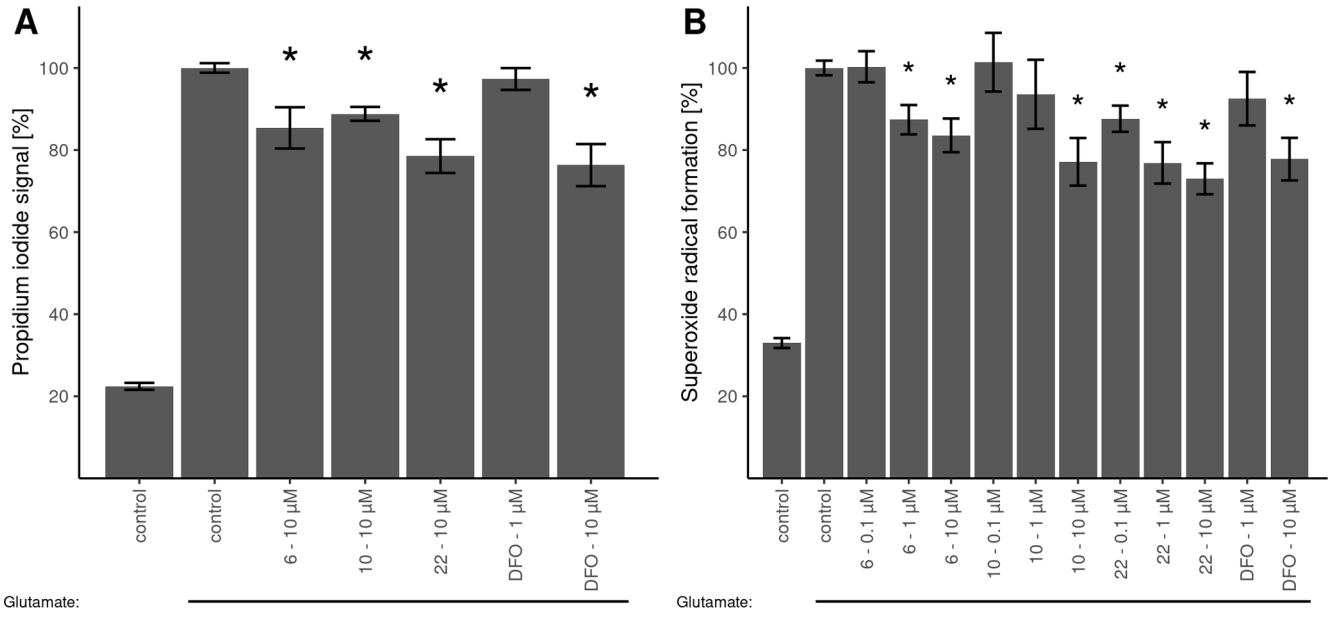

Fig. 5. Protective effects of selected kinetin isosters on glutamate-induced death (panel A) and oxidative stress (panel B) of SH-S5Y5 from ATCC collection. DFO – deferoxamine.

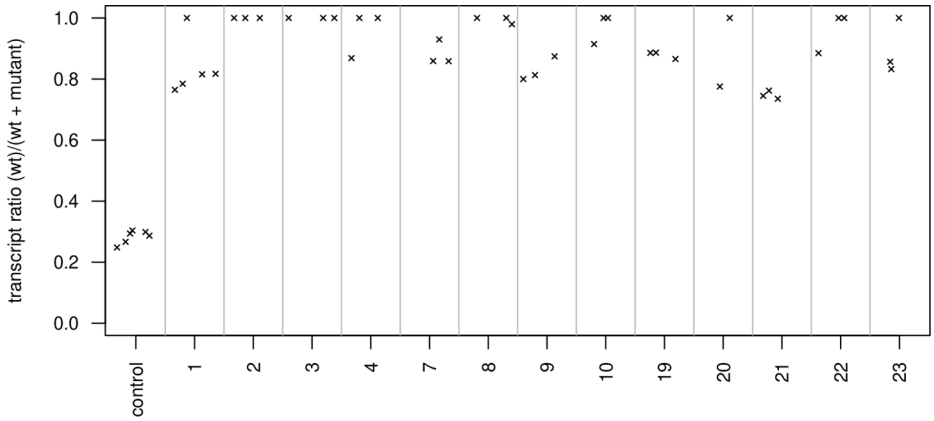

Fig. 6. Effects of the selected isosteres on alternative splicing of mutant ELP1 transcript: wild-type (wt)/wild-type + mutant transcript ratios.

deaza derivatives is also reported in US patent 10676475,[23] where a dual color luminiscence-based reporter system was used for the effect quantification. Activity can also be retained if the imidazole ring is replaced by other 5-membered heterocycles like furan (compound **21**) and thiophene (compound **19** and **20**). On the other hand, 8-aza (compound **11**) and 9-deaza-8-aza (compound **13**) derivatives were inactive. 7-deaza-8-azapurine derivatives substituted by a methyl group at position 9, the N^6-nitrogen or furan ring (compounds **15**–**18**) were also inactive. The binding site of the unknown target can accommodate even larger substituents, as demonstrated by the activity of the derivatives where the imidazole is replaced by either furan ring substituted by two methyl groups (compound **22**) or benzene (compound **23**). It has already been reported that the 2-chloro derivative of kinetin is an even more potent regulator of ELP1 splicing.[20] Similarly, 2-chloro- derivatives (where available) in our series of compounds retained the activity of their unsubstituted parent compounds.

3.5. *In vitro ADME assays*

Kinetin (**1**), 2-chlorokinetin (**2**) and their isosteres **3**–**13** and **19**–**23** were subjected to biochemical assays that can be used to predict absorption, distribution, metabolism and excretion (ADME) properties.[56,57] The compounds selected for these assays excluded methylated derivatives, except **22**, where the substitution is on the purine ring.

The parallel artificial membrane permeability assay (PAMPA),[58] which measures compounds' permeation across hexadecane membranes, was used to estimate the selected compounds' absorption by passive diffusion. For this, we assessed their rates of transport across Caco-2 (human colon carcinoma cells with transport properties similar to enterocytes) and MDCK-MDR1 (dog kidney cells expressing a human efflux transporter) monolayers, which are reliable predictors of compounds' ability to cross intestinal[38] and blood-brain barriers (BBB)[37], respectively. Both apical-to-basal and basal-to-apical movements through the barriers were studied, in efforts to identify compounds that are subject to active efflux. Metabolization by human plasma and liver microsomal fractions was used to evaluate the selected compounds' stability. Finally, binding of the compounds to human plasma proteins was studied. The results of all the assays are summarized in Fig. 7.

The compounds showed good plasma stability (83–100% remaining after 2 h incubation) and most of them also had good microsomal stability (median 78% remaining after 1 h incubation). Degradation exceeded 50% only in two cases: **20** and **22.** Compound **22** was particularly prone to degradation, possibly because of the dimethyl

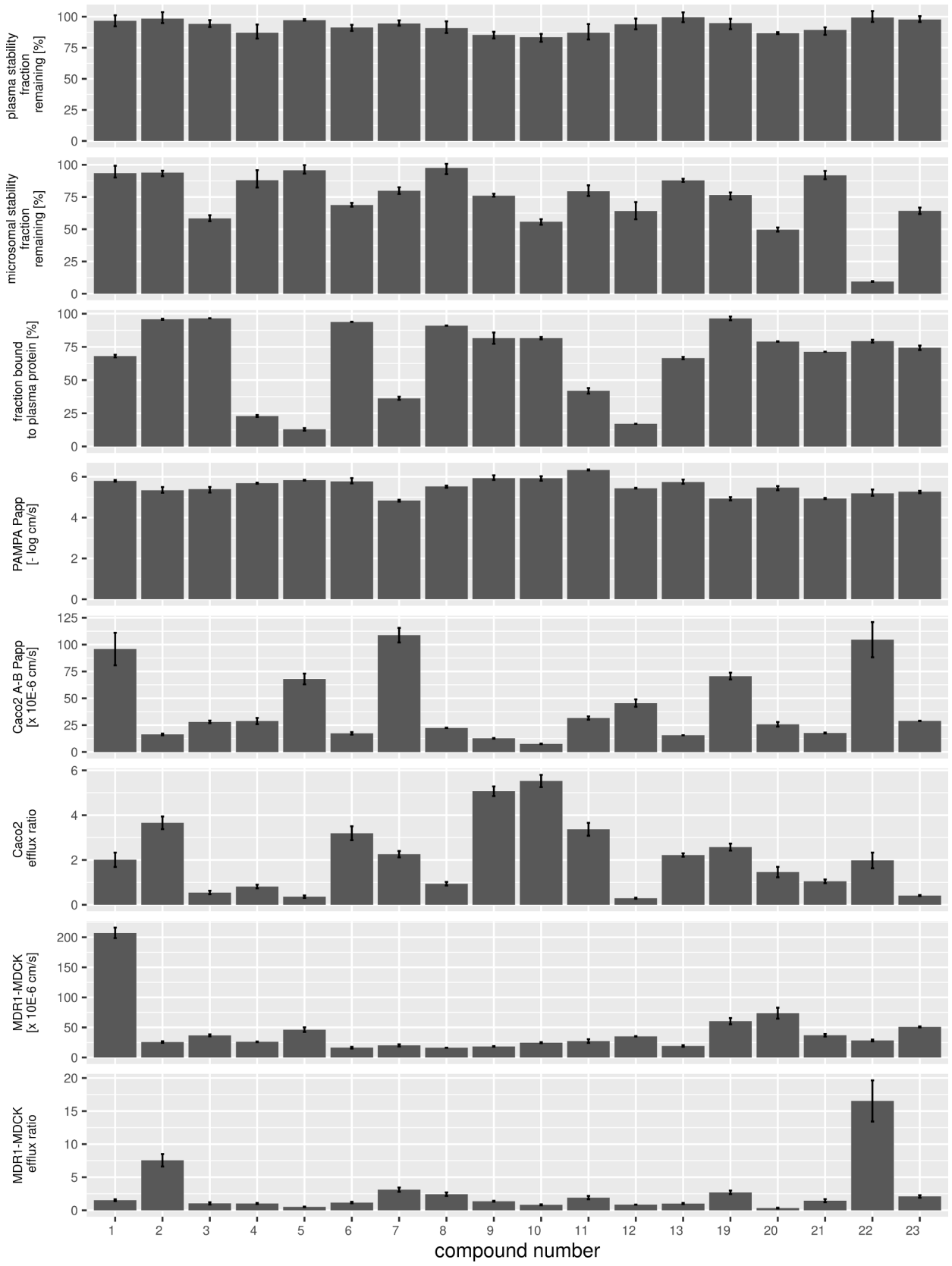

Fig. 7. Overview of the results of ADME *in vitro* assays. Error bars are ranges of values (triplicates in biochemical assays, duplicates in cell-based permeability assays). Standard errors calculated by the Delta method[40]) are only given for results of efflux ratio experiments.

substitution on the 5-membered ring of the purine moiety. Plasma protein binding was highly variable (12.9–96.6%, median 76.7%). Results of the PAMPA assays (log Papp −6.3 to −4.8 cm/s, 1st quartile −5.8 cm/s, median −5.5 cm/s, 3rd quartile −5.3 cm/s) indicate that majority of compounds can readily cross biological barriers by passive diffusion. Compounds with log Papp > −6 cm/s are classified as having high permeability. Results of the Caco-2 and MDCK-MDR1 assays (Papp = 7.6–108.8 and 16.3–207.3 in the units of 10^{-6} cm/s, respectively) are substantially higher than thresholds for high oral absorbance (5×10^{-6} cm/s) and BBB penetration (10×10^{-6} cm/s). Remarkably high values were obtained for kinetin, suggesting possible facilitated transport across the cell membrane. Comparably high absorption was observed for **5, 7, 19** and **22** in Caco-2, but not MDCK-MDR1 cells. The reason for this difference is unclear, although differences in the abundance and/or types of membrane transporters present could be responsible. Differences in compounds' efflux rates could also contribute to this effect, as three of these compounds are among those with the highest efflux rates from MDCK-MDR1 cells. However, compound fluxes are influenced by complex interactions of multiple factors, which would require substantial further elucidation.

3.6. Conclusion

Kinetin has been proposed as a potential therapeutic for diverse conditions and promotion of healthy aging (reviewed by Kadlecová et al. in 2019[2]). It even reached clinical trials for treating skin photoaging[59] and familial dysautonomia[7]. However, few previous peer reviewed studies have assessed pharmacological activities of kinetin derivatives[20–22], and none of them explored effects of modifications of the purine ring system. Some purine isosters are revealed in patent literature, however.[23,24]

Here, we report the pharmacological activity of kinetin and 2-chlorokinetin purine isosteres, and show that some of them have activities not reported for the parent compounds. For example, compound 6 was originally identified as a compound that can protect FA fibroblasts against oxidative stress in our previously mentioned, unpublished high-throughput campaign. The same compound, together with several others, also protected neuron-like cells against oxidative stress damage after high dose glutamate treatment. It would be interesting to evaluate those compounds in other models of mitochondrial and neurodegenerative diseases.

To our disappointment, compound 6 did not correct aberrant splicing of ELP1 transcripts. It would be advantageous to have a compound with such combined activity for treating familial dysautonomia, where stress contributes to the neurodegeneration progression. Overall, activity in the splicing assay was most tolerant of isosteric replacement in the purine core. This tolerance was remarkable in the case of the 5-membered ring, suggesting that it faces toward the cytosolic part of the unknown target's binding site.

We anticipate that isosteric purine replacement could be beneficial not only for improving kinetin's activity toward some targets by increasing interaction with the binding sites but also for increasing the safety of the treatment by limiting affinity for off-targets. This may be particularly important for a compound such as kinetin that has adenine moiety that is present in many important regulatory and signaling molecules. A lower propensity to interact with the purinome generally is thus clearly a desirable property in most cases. Although molecular targets of kinetin remain mostly elusive, it seems highly unlikely that the wide range of reported activities is mediated by a single target or pathway. Kinetin isosteres could therefore also be used for studies of the independence of its various activities. Isosteric replacement also modulates pharmacokinetic properties. Although our data suggest that majority of kinetin isosteres can reach CNS after oral administration, they also show that replacement of the purine ring system of kinetin may result in reduced bioavailability, making development of derivatives with the better activity in the target tissues more difficult. We conclude that isosteric replacement of kinetin's purine moiety is a fruitful strategy for not only improving its known activities but also for exploring therapeutic applications.

Declaration of Competing Interest

The authors declare that they have no known competing financial interests or personal relationships that could have appeared to influence the work reported in this paper.

Acknowledgement

Funding: This work was supported by the Ministry of Education, Youth and Sports of the Czech Republic (INTER-COST project [grant number LTC18078]), European Structural and Investment Funds, Operational Programme Research, Development and Education – project "Preclinical Progression of New Organic Compounds with Targeted Biological Activity" (Preclinprogress) [grant number CZ.02.1.01/0.0/0.0/16_025/0007381] and the European Regional Development Fund – project ENOCH [grant number CZ.02.1.01/0.0/0.0/16_019/0000868]. The collaboration of the Czech and French teams was realized within the frame of COST Action CA15133 (FeSBioNet). The authors are grateful to Kateřina Faksová, Dita Jordová and Marianna Rózsa for their excellent technical assistance.

Appendix A. Supplementary material

Supplementary data to this article can be found online at https://doi.org/10.1016/j.bmc.2021.115993.

References

1 Voller J, Maková B, Kadlecová A, Gonzalez G, Strnad M. Plant hormone cytokinins for modulating human aging and age-related diseases. In: Rattan S, Sharma R, eds. *Hormones in Ageing and Longevity. Healthy Ageing and Longevity*6.
2 Kadlecová A, Maková B, Artal-Sanz M, Strnad M, Voller J. The plant hormone kinetin in disease therapy and healthy aging. *Age Res Rev*. 2019;55:100958. https://doi.org/10.1016/j.arr.2019.100958.
3 Rattan SI, Clark BF. Kinetin delays the onset of ageing characteristics in human fibroblasts. *Biochem Biophys Res Commun*. 1994;201:665–672.
4 Barciszewski J, Siboska GE, Pedersen BO, Clark BFC, Rattan SIS. A mechanism for the in vivo formation of N6-furfuryladenine, kinetin, as a secondary oxidative damage product of DNA. *FEBS Lett*. 1997. https://doi.org/10.1016/S0014-5793(97)01037-5.
5 Slaugenhaupt SA, Mull J, Leyne M, et al. Rescue of a human mRNA splicing defect by the plant cytokinin kinetin. *Hum Mol Genet*. 2004;13:429–436. https://doi.org/10.1093/hmg/ddh046.
6 Pros E, Fernández-Rodríguez J, Benito L, et al. Modulation of aberrant NF1 pre-mRNA splicing by kinetin treatment. *Eur J Hum Genet*. 2010;18:614–617. https://doi.org/10.1038/ejhg.2009.212.
7 Axelrod FB, Liebes L, Gold-von Simson G, et al. Kinetin improves IKBKAP mRNA splicing in patients with familial dysautonomia. *Pediatr Res*. 2011;70:480–483.
8 Yannai S, Zonszain J, Donyo M, Ast G. Combinatorial treatment increases IKAP levels in human cells generated from Familial Dysautonomia patients. *PLoS One*. 2019;14. https://doi.org/10.1371/journal.pone.0211602.
9 Hertz NT, Berthet A, Sos ML, et al. A neo-substrate that amplifies catalytic activity of parkinson's-disease- related kinase PINK1. *Cell*. 2013;154:737–747. https://doi.org/10.1016/j.cell.2013.07.030.
10 Bowie LE, Maiuri T, Alpaugh M, et al. N6-Furfuryladenine is protective in Huntington's disease models by signaling huntingtin phosphorylation. *PNAS*. 2018;115:E7081–E7090.
11 Werner T, Schmülling T. Cytokinin action in plant development. *Curr Opin Plant Biol*. 2009;12:527–538.
12 Doležal K, Popa I, Hauserová E, et al. Preparation, biological activity and endogenous occurrence of N6-benzyladenosines. *Bioorg Med Chem*. 2007;15:3737–3747.
13 Colombo F, Falvella FS, De Cecco L, et al. Pharmacogenomics and analogues of the antitumour agent N 6 -isopentenyladenosine. *Int J Cancer*. 2009;124:2179–2185.
14 Ottria R, Casati S, Maier JAM, Mariotti M, Ciuffreda P. Novel isopentenyladenosine analogues: synthesis, characterization, and evaluation of antiproliferative activity on bladder carcinoma cells. *Nucleosides Nucleotides Nucleic Acids*. 2009;28:736–751. https://doi.org/10.1080/15257770903155550.
15 Ottria R, Casati S, Baldoli E, Maier JAM, Ciuffreda P. N6-Alkyladenosines: synthesis and evaluation of in vitro anticancer activity. *Bioorg Med Chem*. 2010;18:8396–8402. https://doi.org/10.1016/j.bmc.2010.09.030.
16 Amiable C, Pochet S, Padilla A, Labesse G, Kaminski PA. N6-substituted AMPs inhibit mammalian deoxynucleotide N-hydrolase DNPH1. Fraidenraich D, ed. *PLoS One*. 2013;8. https://doi.org/10.1371/journal.pone.0080755.

17 Castiglioni S, Ciuffreda P, Casati S, Ottria R, A.M. Maier J. N6-Isopentenyladenosine and its analogue n6-benzyladenosine induce cell cycle arrest and apoptosis in bladder carcinoma T24 cells. *Anticancer Agents Med Chem*. 2013;13:672–678. https://doi.org/10.2174/1871520611313040016.

18 Oslovsky VE, Drenichev MS, Alexeev CS, Solyev PN, Esipov RS, Mikhailov SN. Synthesis of Cytokinins via Enzymatic Arsenolysis of purine nucleosides. *Curr Protoc Nucleic Acid Chem*. 2018;75. https://doi.org/10.1002/cpnc.61.

19 Matušková V, Zatloukal M, Voller J, et al. New aromatic 6-substituted 2′-deoxy-9-(β)-d-ribofuranosylpurine derivatives as potential plant growth regulators. *Bioorg Med Chem*. 2020;28:115230. https://doi.org/10.1016/j.bmc.2019.115230.

20 Yoshida M, Kataoka N, Miyauchi K, et al. Rectifier of aberrant mRNA splicing recovers tRNA modification in familial dysautonomia. *PNAS*. 2015;112:2764–2769.

21 Salani M, Urbina F, Brenner A, et al. Development of a screening platform to identify small molecules that modify ELP1 Pre-mRNA splicing in familial dysautonomia. *SLAS Disc: Adv Sci Drug Disc*. 2019;24:57–67.

22 Hönig M, Plíhalová L, Spíchal L, et al. New cytokinin derivatives possess UVA and UVB photoprotective effect on human skin cells and prevent oxidative stress. *Eur J Med Chem*. 2018;150:946–957. https://doi.org/10.1016/j.ejmech.2018.03.043.

23 Slaugenhaupt SA, Johnson G, Paquette WD, Zhang W, Marugan J. *United States Patent: 10676475 – Compounds for improving mRNA splicing*. 2020.

24 de Roulet, DeVita. *United States Patent: 10167286 – Compositions and methods using the same for treatment of neurodegenerative and mitochondrial disease*. 2019.

25 Davoll J. 26. Pyrrolo[2,3-d]pyrimidines. *J Chem Soc*. 1960:131–138. https://doi.org/10.1039/JR9600000131.

26 Weiss R, Robins RK, Noell CW. Potential purine antagonists. XXIII. Synthesis of some 7-substituted amino-v-triazolo(d)pyrimidines1. *J Org Chem*. 1960:765–770. https://doi.org/10.1021/jo01075a023.

27 Rogozińska JH, Kroon C, Salemink CA. Influence of alterations in the purine ring on biological activity of cytokinins. *Phytochemistry*. 1973;12:2087–2092.

28 Savelieva EM, Oslovsky VE, Karlov DS, et al. Cytokinin activity of N6-benzyladenine derivatives assayed by interaction with the receptors in planta, in vitro, and in silico. *Phytochemistry*. 2018;149:161–177.

29 Kubiasová K, Mik V, Nisler J, et al. Design, synthesis and perception of fluorescently labeled isoprenoid cytokinins. *Phytochemistry*. 2018;150:1–11.

30 Robins RK, Furcht FW, Grauer AD, Jones JW. Potential purine antagonists. II. Synthesis of some 7- and 5,7-substituted pyrazolo [4,3-d]pyrimidines. *J Am Chem Soc*. 1956;78:2418–2422. https://doi.org/10.1021/ja01592a021.

31 Gervason S, Larkem D, Mansour AB, et al. Physiologically relevant reconstitution of iron-sulfur cluster biosynthesis uncovers persulfide-processing functions of ferredoxin-2 and frataxin. *Nat Commun*. 2019;10. https://doi.org/10.1038/s41467-019-11470-9.

32 Stone JS, Shang J-L, Tomarev S. Expression of Prox1 defines regions of the avian otocyst that give rise to sensory or neural cells. *J Comp Neurol*. 2003;460:487–502.

33 Carrasco RA, Stamm NB, Patel BKR. One-step cellular caspase-3/7 assay. *Biotechniques*. 2003;34:1064–1067.

34 Kim MS, Seo JY, Oh J. Neuroprotective effect of halophyte Salicornia herbacea L. is mediated by activation of heme oxygenase-1 in mouse hippocampal HT22 cells. *J Med Food*. 2017;20:140–151.

35 Anderson SL, Qiu J, Rubin BY. EGCG corrects aberrant splicing of IKAP mRNA in cells from patients with familial dysautonomia. *Biochem Biophys Res Commun*. 2003;310:627–633.

36 Borková L, Frydrych I, Jakubcová N, et al. Synthesis and biological evaluation of triterpenoid thiazoles derived from betulonic acid, dihydrobetulonic acid, and ursonic acid. *Eur J Med Chem*. 2020;185:111806. https://doi.org/10.1016/j.ejmech.2019.111806.

37 Irvine JD, Takahashi L, Lockhart K, et al. MDCK (Madin-Darby Canine Kidney) cells: a tool for membrane permeability screening. *J Pharm Sci*. 1999;88:28–33.

38 Artursson P, Palm K, Luthman K. Caco-2 monolayers in experimental and theoretical predictions of drug transport. *Adv Drug Deliv Rev*. 2001;46:27–43. https://doi.org/10.1016/S0169-409X(00)00128-9.

39 Hammer O, Harper D, Ryan P. PAST: paleontological statistics software package for education and data analysis. *Palaeontol Electron*. 2001;4:1–9.

40 Wu J. Statistical inference for tumor growth inhibition T/C ratio. *J Biopharm Stat*. 2010;20:954–964.

41 Lemrová B, Smyslová P, Popa I, et al. Directed solid-phase synthesis of trisubstituted imidazo[4,5- c]pyridines and imidazo[4,5- b]pyridines. *ACS Comb. Sci*. 2014;16:558–565.

42 Vanda D, Soural M, Canale V, et al. Novel non-sulfonamide 5-HT 6 receptor partial inverse agonist in a group of imidazo[4,5- b]pyridines with cognition enhancing properties. *Eur J Med Chem*. 2018;144:716–729.

43 Bürk K. Friedreich Ataxia: current status and future prospects. *Cerebellum Ataxias*. 2017;4:1–9. https://doi.org/10.1186/s40673-017-0062-x.

44 Richardson TE, Yang S-H, Wen Y, Simpkins JW. Estrogen protection in Friedreich's Ataxia skin fibroblasts. *Endocrinology*. 2011;152:2742–2749. https://doi.org/10.1210/en.2011-0184.

45 Richardson TE, Simpkins JW. R- and S-Equol have equivalent cytoprotective effects in Friedreich's Ataxia. *BMC Pharmacol Toxicol*. 2012;13:12. https://doi.org/10.1186/2050-6511-13-12.

46 Ferriero R, Manco G, Lamantea E, et al. Phenylbutyrate therapy for pyruvate dehydrogenase complex deficiency and lactic acidosis. *Sci Transl Med*. 2013;5. https://doi.org/10.1126/scitranslmed.3004986.

47 Bonnier F, Keating ME, Wróbel TP, et al. Cell viability assessment using the Alamar blue assay: a comparison of 2D and 3D cell culture models. *Toxicol In Vitro*. 2015;29:124–131. https://doi.org/10.1016/j.tiv.2014.09.014.

48 Pastore A, Puccio H. Frataxin: a protein in search for a function. *J Neurochem*. 2013;126:43–52.

49 Ali A, Zhang Q, Dai J, Huang X. Calcein as a fluorescent iron chemosensor for the determination of low molecular weight iron in biological fluids. *Biometals*. 2003;16:285–293. https://doi.org/10.1023/A:1020642808437.

50 Xicoy H, Wieringa B, Martens GJM. The SH-SY5Y cell line in Parkinson's disease research: a systematic review. *Mol Neurodegener*. 2017;12:1–11. https://doi.org/10.1186/s13024-017-0149-0.

51 Kritis AA, Stamoula EG, Paniskaki KA, Vavilis TD. Researching glutamate – induced cytotoxicity in different cell lines: a comparative/collective analysis/study. *Front Cell Neurosci*. 2015;9:91. https://doi.org/10.3389/fncel.2015.00091.

52 Ito K, Eguchi Y, Imagawa Y, Akai S, Mochizuki H, Tsujimoto Y. MPP+ induces necrostatin-1-and ferrostatin-1-sensitive necrotic death of neuronal SH-SY5Y cells. *Cell Death Discov*. 2017;3:1–10. https://doi.org/10.1038/cddiscovery.2017.13.

53 Kulikov AV, Rzhaninova AA, Goldshtein DV, Boldyrev AA. Expression of NMDA receptors in multipotent stromal cells of human adipose tissue under conditions of retinoic acid-induced differentiation. *Bull Exp Biol Med*. 2007;144:626–629. https://doi.org/10.1007/s10517-007-0390-6.

54 Nishida Y, Adati N, Ozawa R, et al. Identification and classification of genes regulated by phosphatidylinositol 3-kinase- and TRKB-mediated signalling pathways during neuronal differentiation in two subtypes of the human neuroblastoma cell line SH-SY5Y. *BMC Res Notes*. 2008;1:95. https://doi.org/10.1186/1756-0500-1-95.

55 Slaugenhaupt SA, Blumenfeld A, Gill SP, et al. Tissue-specific expression of a splicing mutation in the IKBKAP gene causes familial dysautonomia. *Am J Hum Genet*. 2001;68:598–605. https://doi.org/10.1086/318810.

56 Di L, Kerns EH. Profiling drug-like properties in discovery research. *Curr Opin Chem Biol*. 2003;7:402–408. https://doi.org/10.1016/S1367-5931(03)00055-3.

57 Zhang D, Luo G, Ding X, Lu C. Preclinical experimental models of drug metabolism and disposition in drug discovery and development. *Acta Pharmaceutica Sinica B*. 2012;2:549–561. https://doi.org/10.1016/j.apsb.2012.10.004.

58 Yu H, Wang Q, Sun Y, et al. A new PAMPA model proposed on the basis of a synthetic phospholipid membrane. Hofmann A, ed. *PLoS One*. 2015;10. https://doi.org/10.1371/journal.pone.0116502.

59 Wanitphakdeedecha R, Meeprathom W, Manuskiatti W. Efficacy and safety of 0.1% kinetin cream in the treatment of photoaging skin. *Indian J Dermatol Venereol Leprol*. 2015;81:547. https://doi.org/10.4103/0378-6323.157446.